A MICROFLUIDIC CHIP FOR PULMONARY ARTERIAL HYPERTENSION

Beata Wojciak-Stothard (b.wojciak-stothard@imperial.ac.uk)
Imperial College London https://orcid.org/0000-0002-6607-7372
Alexander Ainscough
Imperial College London
Timothy Smith
Imperial College London
Christopher Rhodes
Imperial College London
Adam Fellows
Imperial College London
Luke Howard
Imperial College London
John Wharton
Imperial College London
Martin Wilkins
Imperial College London
Joshua Edel
Imperial College London https://orcid.org/0000-0001-5870-8659

Article

Keywords:

Posted Date: June 7th, 2021

DOI: https://doi.org/10.21203/rs.3.rs-598765/v1

Abstract

Pulmonary arterial hypertension (PAH) is an unmet clinical need. The lack of a disease model representative of the human condition is a key obstacle to the development of new treatments. Here we present a model of PAH, based on a biomimetic pulmonary artery (PA)-on-a-chip, that permits the study of the molecular and functional changes in human pulmonary vascular endothelial and smooth muscle cells in response to triggers of the disease and their response to drugs. We combine natural or induced BMPR2 dysfunction with hypoxia in vascular endothelial cells to trigger smooth muscle activation and proliferation and relate accompanying transcriptomic changes in affected cells to functional effects. Changes in gene expression consistent with observations made in genomic and biochemical studies of the human disease enable insights into underlying disease pathways and mechanisms of drug response. The model offers a novel, promising and more easily accessible approach for researchers to study pulmonary vascular remodelling and advance drug development in PAH.

Introduction

Pulmonary arterial hypertension (PAH) is a progressive disease of the pulmonary circulation characterised by narrowing of pulmonary arteries and arterioles, leading to the right heart hypertrophy and heart failure[1]. Endothelial damage is an early event, which triggers proliferation of cells in the arterial intimal and medial layers[2]. Endothelial-to-mesenchymal transition is well documented and changes in vascular cell phenotype include aerobic glycolysis and conversion of pulmonary vascular smooth muscle cells from the differentiated, contractile phenotype to a proliferating, synthetic phenotype [3]. Existing drugs bring some symptomatic relief but, in most patients, do not arrest or reverse the disease[4].

Rare genetic mutations have been identified that increase susceptibility to PAH, which can be initiated by other factors, such as hypoxia and inflammation[5]. A key genetic change increasing susceptibility to PAH is a heterozygous germline mutation in the gene encoding the bone morphogenetic protein type II receptor (*BMPR2*). Over 300 have been identified and studies report *BMPR2* mutations in over 80% of cases of familial PAH, and around 20% of sporadic or idiopathic PAH patients [6]. Non-genetic forms of PAH show reduced expression and increased degradation of the receptor[7]. While mutations in *BMPR2* and other TGF-β receptor superfamily member genes account for most cases of heritable PAH*,* other genes and genetic loci have been linked with the condition[6,8].

Animal models are used to aid our understanding of basic disease mechanisms and evaluate the efficacy of drug treatments but these models do not fully reproduce the arteriopathy seen in the patient with PAH[9]. Organs-on-chips have emerged in the last decade as a technology with huge potential to revolutionise *in vitro* disease modelling and increase the accuracy and throughput of pharmacological and toxicological screening. In addition, there is the potential to personalise medicine development through the use of stem cell derived cells including patient-derived induced pluripotent stem cells and endothelial colony forming cells (ECFCs).

Here, we present a microfluidic model of PAH in a pulmonary artery-on-a-chip, capable of reproducing disease characteristics within 48h of culture. In a series of carefully controlled steps, we first validate the device as a model of a live vessel and then characterise functional and transcriptomic changes in endothelial and smooth muscle cells induced by a combination of BMPR2 knockdown and hypoxia. The resultant changes constitute a signature of the disease and we show that they are inhibited by imatinib, a tyrosine kinase inhibitor, with therapeutic potential in patients with PAH[10]. The findings are validated with the use of cells from PAH patients with disabling *BMPR2* mutations and comparative analysis of transcriptomic data from human PAH.

Results

Pulmonary artery-on-a-chip reconstitutes features of human lung arteries

The pulmonary artery-on-a-chip (PA-on-a-chip) was designed to monitor responses of human pulmonary vascular cells to pathological and potential therapeutic interventions. The polydimethylsiloxane (PDMS)-based device comprises two microfluidic channels (200μm height x 1000μm width) separated by a nanoporous polyethylene terephthalate (PET) membrane, with human pulmonary artery endothelial cells (HPAECs) and human pulmonary artery smooth muscle cells (HPASMCs) cultured on either side of the membrane **(Fig.1a, b**). Membrane porosity (pore size 400 nm, density $2x10^6$ pores/cm^2) enables direct communication between cells, reflective of the role of basal lamina in pulmonary arteries[11,12]. Inlets and outlets of endothelial channels are connected with tubing and pulse dampeners, to allow circulation of culture medium, actuated by a laminar shear stress under physiological flow rates of 6 dynes/cm^2, characteristic of human lung arterioles[13] (**Fig 1c, d and Supplementary Figures S1-S3**). Basic principles of the design were based on the lung-on-a-chip model[14].

HPAECs aligned within the direction of flow, whereas HPASMCs exhibited a tendency for perpendicular orientation, reminiscent of the arterial intimal and medial cell configurations *in vivo* (**Figure 1e-h**). Flow-stimulated HPAECs showed enhanced junctional localization of vascular endothelial (VE)-cadherin and significantly elevated expression of endothelial maturity markers PECAM-1 and KLF2 (**Figure 1h-j**). The functionality of endothelial barrier was evaluated by measuring the passage of fluorescently-labelled 40kDa dextran, which has a Stokes radius similar to human plasma albumin[15], across the endothelial and smooth muscle layers stimulated with thrombin, a known vasoconstrictor and permeability factor [16]. HPAECs grown in PA-on-a-chip showed a ~5-fold decrease in basal endothelial permeability, compared with static controls (**Figure 1k**). This is reflective of endothelial function *in vivo*, where cells under dynamic flow conditions form a tighter barrier compared with cells in traditional static cell culture models[17]. HPAECs in PA-on-a-chip also showed a markedly larger increase in thrombin-induced permeability over baseline, compared with unstimulated controls (3.9-fold increase in PA-on-a-chip vs 1.5-fold increase in static culture) (**Figure 1k**). HPASMCs had no significant effect on endothelial barrier function under study conditions (**Supplementary Figure S4**).

Establishment of a PAH model on-a-chip

Remodelled PAH vasculature is characterised by intimal and medial thickening (**Figure 2a, b**). There is a significant need to understand how endothelial *BMPR2* haploinsufficiency, in combination with the "second hit" created by hypoxia or inflammation, elicits disease.

To recreate disease conditions in the PA-on-a-chip, HPAECs infected with AdBMPR2 shRNA were exposed to hypoxia (2% O_2) for 24h. The adenoviral infection was optimised to achieve ~50% reduction in BMPR2 expression, reflective of BMPR2 haploinsufficiency in PAH (**Fig 2c**).

BMPR2 knockdown and hypoxia, separately and in combination, under the conditions of flow in the microfluidic model did not affect endothelial permeability or proliferation (**Figure 2d and Supplementary Figure S5A**), in contrast with the observations in static cell culture[18]. HPASMC proliferation was significantly increased when knockdown and hypoxia were combined ($P<0.01$; **Fig 2e**). This response was inhibited by treatment with 10μM imatinib mesylate, a receptor tyrosine kinase inhibitor currently under investigation as an anti-proliferation treatment of PAH ($P<0.05$; **Fig 2e**). No significant loss of cells from endothelial or smooth muscle channels was noted (**Supplementary Figures S5 B, C**).

Genotype- and oxygenation-specific transcriptomic signatures from the "double hit" microfluidic model of PAH.

Control and BMPR2-deficient HPAECs co-cultured with HPASMCs under normoxic or hypoxic conditions underwent RNAseq analysis to identify key transcriptomic changes. *BMPR2* knockdown alone induced differential expression of 1828 genes, compared to control conditions, in HPAECs (logFC>0.25, $P<0.05$), where a reduction in BMPR2 expression was the most significant change (-2.9-fold change, $p=2.07x10^{-9}$) (**Figure 2f)**. These genes showed enrichment in epithelial-to-mesenchymal transition (EMT), G2M checkpoint, myc targets, cell cycle (E2F targets) and DNA repair pathways (Hallmark, FDR<0.01). HPASMCs co-cultured with BMPR2-deficient HPAECs showed differential expression of 751 genes (**Supplementary Figure S6),** associated predominantly with hypoxia, glycolysis, EMT and cholesterol homeostasis (Hallmark, FDR<0.01)

The combination of BMPR2 knockdown with hypoxia induced differential expression of 1090 genes in HPAECs and 895 genes in HPASMCs. The pattern of these changes is illustrated in volcano plots (**Figure 2g, h)** and heatmaps showing distinct hypoxia-, genotype- and "double hit"-related gene clustering **(Supplementary Figure S7**). A list of differentially expressed genes (DEG) in HPAEC and HPASMCs in the "double hit" model of PAH is provided in the **Supplementary File S1**.

Transcriptional profiling of HPAECs from the "double hit" model identified multiple genes linked with known PAH pathways, including TGF-β signalling, NOS pathway, proliferation, angiogenesis, Notch signalling, EndoMT, ion channels, fibrosis and inflammation (**Figure 3a and Supplementary Figure S8A**). ~80% of the observed changes could be attributed to *BMPR2* knockdown, including the downregulation of genes in TGF-β, NOS signaling pathway, junctional proteins and growth factor signalling mediators.

Additional exposure of BMPR2-deficient cells to hypoxia altered the expression of genes predominantly linked to glycolysis, cell cycle, DNA repair and TNF-α signalling. DEG induced by hypoxia in BMPR2-deficient HPAECs and the corresponding GSEA pathway analysis data are provided in **Supplementary Files S2 and S3.**

HPASMCs in the "double hit" PAH model showed associations with several pathways involved in vascular remodelling, including angiogenesis, apoptosis, inflammation, vasoconstriction and TGF-β signaling (**Figure 3b, Supplementary Figure S8B**). Only ~30% of these changes could be attributed to endothelial *BMPR2* knockdown. The additional genes affected by hypoxic exposure were linked to glycolysis, adipogenesis, TNF-α, cell cycle, Rho signalling and ECM interactions. DEG affected by HPAEC *BMPR2* silencing in normoxic HPAECs and HPASMCs are provided in the **Supplementary File S4**. Hypoxia-regulated HPASMC genes in the "double hit" model and the corresponding GSEA pathway analysis data are provided in **Supplementary Files S2 and S5**, respectively**.**

Changes in the expression of selected HPAEC and HPASMC gene targets were validated by qPCR (**Supplementary Figure S9**)

Model validation with PAH cells with *BMPR2* mutations

Blood-derived endothelial colony-forming cells (ECFCs) are often used as surrogates for pulmonary endothelial cells in PAH and display abnormalities in key pathways linked to the disease pathogenesis[19,20]. It is thought that ECFCs may facilitate the formation of occlusive angio-proliferative vascular lesions in PAH[21].

To investigate whether the effects seen in the "double hit" model of PAH would yield similar findings in patient-derived cells, we opted to substitute HPAECs with ECFCs from PAH patients with disabling *BMPR2* mutations. The process of isolation and culture of ECFCs is illustrated in **Fig 4a**. PAH ECFCs did not show major morphological or functional differences with healthy controls (**Figure 4b, c and Supplementary Figure S10**). Consistent with the responses seen in the "double hit" PAH model, HPASMCs co-cultured with PAH ECFCs under hypoxic conditions showed a significant ~2-fold increase in proliferation (**Figure 4d).** No changes in ECFC and HPASMC apoptosis were observed **(Supplementary Figure S11)**

Despite the lack of morphological differences between PAH ECFCs and healthy controls, normoxic PAH ECFCs with *BMPR2* mutations showed 1065 differentially expressed genes (DEG) (**Figure 4e),** associated predominantly with ROS, KRAS, MTOR signalling and adipogenesis (Hallmark, $p<0.01$). 15% of this gene pool was shared with BMPR2-deficient HPAECs and included key regulators of vascular homeostasis such as *DDAH1, CAV1, PDGFB, KLF2, APLN* (**Supplementary File S6**). HPASMCS co-cultured with PAH ECFCs showed 972 DEG **(Supplementary Figure S12)** enriched in cell cycle progression (E2F targets), G2M checkpoint, oxidative phosphorylation, interferon gamma pathways (Hallmark, FDR<0.01). A list of DEG in BMPR2-deficient ECFCs and HPASMCs co-cultured with these cells under normoxic conditions is provided in the **Supplementary File S7.**

PAH ECFCs from the “double hit” ECFC PAH model (combining PAH BMPR2 mutations and hypoxia) showed 2360 DEG, while HPASMCs showed 689 DEG (logFC>0.25, P<0.05) (**Fig 4f, g and Supplementary File S1)**. Hierarchical gene clustering in ECFCs and HPASMCs under different experimental conditions revealed genotype- and oxygenation-specific changes in gene expression **(Figure 5a, b and Supplementary Figure S13)**

ECFC differentially expressed genes from the “double hit” model showed enrichment in key PAH pathways, including angiogenesis, apoptosis, EMT, fibrosis, inflammation, proliferation, nitric oxide, TGF-β, Notch and Wnt signaling (Hallmark, FDR<0.01) (**Figure 5a and Supplementary Figure S14A).** Only ~30% of these genes were related to *BMPR2* mutation. The remaining ~70% genes induced by additional hypoxic exposure showed links with glycolysis, adipogenesis, cell cycle, oxidative phosphorylation, Rho signalling, TNF-α signalling and cellular senescence **(Supplementary File S8**).

HPASMC genes from the “double hit” ECFC PAH model showed significant associations with angiogenesis, apoptosis, hypoxia, inflammation, proliferation, fibrosis and TGF-β pathways **(Figure 5b and Supplementary Figure S14B)**. 38% of these genes could be related to the BMPR2 loss of function, with 62% of changes affected by hypoxia and linked with glycolysis, pentose metabolism, cell cycle and immune responses. A list of HPASMC genes affected by ECFC *BMPR2* mutations is provided in the **Supplementary File S6**. Hypoxia-regulated genes in these cells and corresponding GSEA pathway analysis data are shown in **Supplementary Files S2 and S9**, respectively.

Transcriptomic overlaps between different PAH datasets

RNAseq datasets from the two microfluidic models of endothelial dysfunction in PAH, utilising either BMPR2-deficient HPAECs or PAH ECFCs with *BMPR2* mutations, were compared with published gene datasets from IPAH lung transplants[22,23] and other gene databases with known PAH associations[24].

Endothelial and smooth muscle DEG from our models and other published datasets are listed in **Supplementary File S10** and the overlapping genes are listed in the **Supplementary File S11**. The results of comparative analysis are shown in **Figure 6a, c.** Heatmaps in **Figure 6b, d** illustrate directional similarities in differential gene expression between the two microfluidic models of PAH described in this study.

The highest number of shared endothelial genes was found between our two microfluidic PAH models (212 genes), between our microfluidic ECFC PAH model and the IPAH PAEC gene dataset (63 genes) and between the “double hit” PAH model and the IPAH PAEC dataset (33 genes) (DisGENET IPAH (https://www.disgenet.org/browser/0/1/0/C3203102/)[24] (**Figure 6a and Supplementary File S11**). GO pathway analysis (Hallmark) of the overlapping endothelial gene datasets revealed their associations with key PAH pathways, including EMT, TNF-α signalling via NFkB, hypoxia, apoptosis, p53 pathway (FDR<0.05) **(Supplementary File S12)**

Consistently, the highest number of shared DE SMC genes was found between our microfluidic PAH models (94 genes), between microfluidic ECFC PAH model and IPAH PASMCs[25] (86 genes) and between the microfluidic "double hit" PAH model and IPAH PASMCs (76 genes) (**Figure 6c and Supplementary File S10**). GO pathway analysis of the overlapping SMC gene datasets highlighted their links with TGF-β signalling, glycolysis, fatty acid metabolism, pentose phosphate pathway, TNF-α via NFκB signalling, cell cycle/G2M checkpoint (FDR <0.05) (**Supplementary File S13**)

Discussion

We present a microfluidic model of PAH that permits the study of dynamic changes in molecular and functional phenotype in relevant cell types under physiological flow conditions in response to key factors linked to the development of the condition, such as *BMPR2* silencing and hypoxia. The model is suitable for the of drugs of potential therapeutic benefit and can accommodate blood-derived endothelial cells from patients, offering the prospective of tailoring medicines to individual patients. Experimental design and key findings are summarised in **Figure 7**.

HPAECs and HPASMCs grown in PA-on-a-chip under physiological levels of shear stress[26,27] showed arterial-like adaptations to flow. Computational modelling of fluid-structure interaction within the channel geometry revealed a uniform, laminar pattern of flow, important in ensuring the data integrity. Although our chip was capable of supporting a long-term cell culture (up to 2 weeks tested), our investigations were carried out within 48 hours, bearing in mind potential applications for drug testing.

Most of *BMPR2* mutation carriers and heterozygous *BMPR2* knockout animals do not spontaneously develop PAH and a "second hit" is required for the full manifestation of the disease[5]. Consistent with this premise, a combination of endothelial *BMPR2* knockdown with hypoxia in PA-on-a-chip was required to induce HPASMC proliferation. HPASMCs were unmodified to gain an understanding of how endothelial dysfunction renders SMCs susceptible to PAH. HPASMC proliferation was prevented by imatinib, a potent inhibitor of platelet-derived growth factor receptor beta (PDGFRβ) and other protein kinases involved in PAH[10]. Demonstration of the effectiveness of imatinib in our model is critical as the drug, evaluated in a phase 3 clinical study (IMPRES), is currently undergoing further trials to establish an efficacious dose amid concerns about its safety and tolerability[28]. BMPR2 knockdown did not affect endothelial barrier function in PA-on-a-chip, in contrast to the observations made in conventional cell culture systems[18]. HPAECs in PA-on-a-chip also showed increased sensitivity to thrombin despite the overall reduction in baseline permeability, which reiterates the importance of testing cell responses under the physiological cell culture conditions.

The mechanisms by which endothelial BMPR2 depletion primes vascular cells for the disease and converges with the effects of the "second hit" are not well understood. Using a combination of functional assays, RNA sequencing and pathway analysis in human pulmonary endothelial and smooth muscle cells and cells from PAH patients with disabling *BMPR2* mutations under the "double hit" conditions, we have identified a "microfluidic signature" of vascular responses characteristic of the disease. Crucially,

this gene dataset showed a substantial overlap with transcriptomic changes reported in in PAH and identified novel gene targets of potential interest.

Loss of BMPR2 in HPAECs inhibited expression of TGF-β family genes involved in vascular differentiation, angiogenesis and vessel maturation[29], including *BMPR2*, *SMAD6* and *SMAD7*[30], *THBS1* (thrombospondin-1)[31], *ID1*[32], *FURIN*,[6] *SMURF2*[33], consistent with changes reported in PAH. HPAECs also showed reduced expression of junctional markers *CDH5* (VE-cadherin), *GJA5* (connexin 40) and several integrins, such as *ITGB1, ITGB3 and ITGB5*, likely to predispose the endothelium to stress-induced damage and abrogate endothelial repair.

BMPR2-deficient HPAECs also showed reduced expression of NO bioavailability enzymes, endothelial nitric oxide synthase (*NOS3)* and dimethylarginine dimethylaminohydrolases 1 and 2 (*DDAH1* and *DDAH2*), consistent with other descriptions of the PAH vasculopathy[35,36]. Other key PAH-related changes included reduction in arterial identity factors *SOX17*[37] and *SOX18*[38], *KLF2*[39] as well as regulators of angiogenesis, proliferation and endothelial sprouting behaviour, such as *KDR*[40], *CAV2*[41], *FGF12*[42], *RhoB*[43], *SHROOM*[44]. Exposure of BMPR2-deficient endothelial cells to hypoxia altered expression of genes controlling oxygen transport, cell cycle, transcriptional regulation and inflammation, including genes with well documented links to PAH: *KCNK3*[45,46], *HDAC4*[47], *BRD4*[48], *CAMK2G*[49,50] and *ICAM1*[51]. To summarise, our “double hit” microfluidic model of PAH offers a snapshot of endothelial changes likely to be seen in early disease, associated with a loss of arterial identity, reduced eNOS signalling and increased susceptibility to damage, accompanied by inflammation and metabolic shift towards glycolysis.

Differential gene expression in HPASMC in the “double hit” PAH model was enriched for disease-specific phenotypes associated with angiogenesis, apoptosis, inflammation, vasoconstriction and TGF-β signalling. 30% of these changes could be attributed to endothelial *BMPR2* knockdown and linked with extracellular matrix remodelling, metabolism, and regulation of the cell cycle. Downregulation of collagens *COL3A1, COL4A1, COL4A2, COL5A1, COL5A2, COL5A3, COL6A1, COL6A2,* as well as *FN1* (fibronectin*), FBN1* (fibrillin-1*), ELN* (elastin), *LAMC2* (laminin subunit gamma 2), *TNC* (tenascin-C)*, SERPINH1* (serpin) and *POSTN* (periostin) and upregulation of matrix metalloproteinases *MMP14* and *MMP15* is likely to reduce arterial structural integrity and stimulate SMC migration and proliferation[52,53]. Loss of *CAV1* (caveolin-1)[54] and *APLN* (apelin)[55] is known to augment vasoconstriction and vascular remodelling in PAH. Downregulation of bone morphogenetic protein *BMP1* and upregulation of *KLF7* can be linked with inhibition of HPASMC apoptosis in PAH[56,57]

Additional exposure of these cells to hypoxia induced changes in glycolysis, adipogenesis, TNF-α and Rho signalling, cell cycle and ECM interactions. Downregulation of cytochrome oxidase assembly regulator, *COX11,* and mitochondrial dehydrogenase, *HSD17B10,* involved in fatty acids metabolism[58], and upregulation of mitochondrial fission protein *MTFP1*[59], pyruvate dehydrogenases *PDK1*[60], *PDK3*[61] and hypoxia-responsive diabetes gene *KLF7*[62,63] have all been linked with mitochondrial dysfunction in PAH. Pro-angiogenic *VEGFA* and pro-survival *VEGFB* and *KLF7* [64] are likely to promote a shift towards

vascular repair, apoptosis resistance and angiogenesis. Another notable change seen in the “double hit” HPASMCs involved reduction in plasmalemmal potassium channels, *KCNMA, KCNAB2, KCNK1*, a change linked with pulmonary vasoconstriction and vascular remodelling[64]. Upregulation of inflammatory genes *RELB*, *CXCL1*, reduction in fibrillar smooth muscle maturity collagens *COL1A2* and *COL1A1*[65,66] and upregulation of pro-migratory and pro-proliferative *COL8A2*[67] creates environment conducive to medial hypertrophy.

Patient blood-derived endothelial colony-forming cells (ECFCs) display abnormalities characteristic of PAH, raising interest in their application in personalised medicine[19,20]. To validate our model, we used patient ECFCs with disabling *BMPR2* mutations in place of BMPR2-depeleted HPAECs. The comparative analysis of cell responses revealed several important similarities but also key differences between the two cell types. Consistent with changes seen in BMPR2-deficient HPAECs, ECFCs with *BMPR2* mutations showed upregulation of inflammatory genes (*IL6, REL, NFKB1, NFKB2, CXCL1, 2, 3, 8, TRAF1, ICAM3*), glycolysis (*HK2, LDHA, PDK4*) and mitochondrial function (*FIS1, STOML2*)[68] and downregulation of key markers of arterial identity (*ERG* and *SOX17*)[69]. However, in contrast with the response seen in HPAECs, ECFCs showed an upregulation of genes regulating NO bioavailability (*NOS3, DDAH1, DDAH2*) and increased expression of genes promoting endothelial repair and angiogenesis (*VEGFA, VEGFB, FGF2, CLIC1, Rac1, ROCK1, ARF6, KLF2, KLF6, KLF7)*.

The ECFCs phenotype seen in our model was consistent with that seen in ECFCs derived from PAH PAECs[70] and is likely to represent endothelial cells in plexiform lesions in the advanced PAH. A link between *BMPR2* and *SOX17/18*, first reported in this study, is intriguing, considering the well documented association of variation in both genes with susceptibility to PAH[6,37].

Our model captures key changes in the pulmonary endothelial phenotype that are essential for the induction of SMC remodelling. Differential gene expression in HPASMCs co-cultured with endothelial cells under the “double hit” conditions showed enrichment for pathways that fuel cell proliferation (GO terms: glycolysis, gluconeogenesis, fatty acid metabolism, pentose phosphate pathway, glycolysis, gluconeogenesis, heme metabolism), inflammation (GO term: TNF-α signalling via NFkB, interferon alpha and gamma response), cell cycle (GO term: cell cycle, G2M checkpoint, myc targets) and apoptosis (GO term: apoptosis, TP53 regulates transcription of cell death genes), consistent with PAH phenotype. The use of blood-derived ECFCs may help identify differences between healthy and IPAH *BMPR2* mutation carriers and facilitate studies on environmental and genetic triggers of the disease.

Economic use of cells, short experimental time, device scalability, low production and operation cost make it an attractive model for drug testing and a viable alternative to animal experimentation. The only other existing PAH-on-a-chip model[71] included intimal, medial and adventitial cells from PAH pulmonary arteries grown on polylysine-coated glass in straight channels arranged side-by-side, with cell-to-cell contact restricted to the gaps between silicone posts situated between the channels. This model can provide valuable information regarding paracrine regulation of cell migration (defined as remodelling *sic*)

but cannot evaluate endothelial barrier function and is limited by poor accessibility of patient lung material, which precludes its wider application in research and drug testing.

The limitations of our model may arise from the innate ability of PDMS to sequester small hydrophobic molecules[72] but these can be addressed by surface modifications and the use of different fabrication materials[73]. Future sourcing of patient-derived cells and introducing other cell types will be a vital consideration as a single microfluidic device, which accommodates only 2-3 different cell types, is unlikely to fully reflect complex pathophysiology of the disease.

In summary, we are first to provide a biomimetic, microfluidic and inducible model of PAH which links functional responses with contemporaneous transcriptional changes in pulmonary BMPR2-depleted human pulmonary endothelial and smooth muscle cells co-cultured under physiological flow conditions and characterise the effects of the hypoxic “second hit”. Significant overlaps of with pre-existing lists of differentially expressed PAH genes, are amenable for novel target discovery/validation and can be applied for use in drug screening or toxicology.

Materials And Methods

PA-on-a-chip simulation

Finite Element Method-based simulations were used to simulate the fluid structure interaction within the PA on-a-chip device using COMSOL Multiphysics version 4.4. A detailed description of the model developed is described in Supplemental Methods.

Photolithography

Individual photomasks were designed for Endothelial and Smooth Muscle Cell chambers using AutoCAD 2017 (Autodesk, CA, USA) and printed on high resolution photomask films (Micro Lithography Services Ltd, UK). Photolithography, soft lithography and pulmonary artery-on-a-chip fabrication were all conducted in an ISO Class 5 Cleanroom (<100,000 particles/m^3). The fabrication procedure was as follows: 100mm diameter single side polished silicon dioxide wafers with resistivity of 1-10 W/cm and thickness of 525mm (Inseto, UK) were sequentially cleaned in isopropanol, acetone and isopropanol again before drying under a gentle stream of N_2 gas followed by dehydration by heating at 95^oC. SU-8 2100 (A-Gas, UK) was spin coated onto the polished surface of the wafer at 1500rpm, corresponding to a 200mm feature height. Wafers were pre-exposure baked on hotplates for 5 minutes at 65^oC and 12 minutes at 95^oC before equilibrating to room temperature. The SU-8 coated wafer was placed inside a UV exposure unit (OAI, CA, USA) containing a 360 nm long pass filter (RS Laser Components, UK) and the appropriate photomask prior to 260mJ/cm^2 UV light exposure. Wafers were baked post-exposure at 65^oC for 5 minutes and 95^oC for 12 minutes on hotplates before developing in Microposit EC Solvent (A-Gas, UK). Developed wafers were placed inside a desiccator along with 35ml of Trichloro(1H,1H,2H,2H-perfluorooctyl)silane (Cat: 448931; Sigma, UK) deposited on a fresh microscope slide. The silane was

vaporised upon evacuation of the desiccator under vacuum conditions and was left to deposit on the wafer surface for 1 hour.

Soft lithography

PDMS (Sylgard 184 Elastomer Kit, Cat: 634165S, Dow Corning, USA) was weighed and mixed at a ratio of 10:1 (base to curing agent) and poured onto SU-8 master moulds. 4-5mm uncured PDMS was poured onto the negative impressions of the SU-8 patterned wafers for the upper (endothelial) compartments and 1-2mm was poured onto SU-8 patterned wafers for the lower (smooth muscle) compartments to enable downstream optical imaging. The mixture was degassed in a desiccator for 1 hour and cured on hotplates for 2 hours at 65^{o}C. PDMS chips were excised using a disposable scalpel, cut to size using a single edge razor blade and had access ports punched using a 0.75mm biopsy punch (Cat: 504529, World Precision Instruments, Hertfordshire, UK).

Pulmonary artery-on-a-chip fabrication

PDMS chips were plasma activated/sterilised for 60 seconds in a plasma cleaner (Harrick Plasma, NY, USA) and immediately immersed in a solution of anhydrous ethanol containing 2.5% GLYMO (Cat: 440167; Sigma Aldrich, Dorset, UK) for 20 minutes at room temperature. Porous PET membranes (0.4µm pores; 2x10^{6} pores/cm^{2}; it4ip, Louvain-la-Neuve, Belgium) were plasma activated/sterilised for 60 seconds, immersed in a solution of anhydrous ethanol containing 10% APTES (Cat: 440140; Sigma Aldrich, Dorset, UK) and heated at 65^{o}C for 20 minutes. Chips and membranes were rinsed in IPA, dried in a stream of N2 gas, manually aligned and brought into conformal contact. Chip bonding was completed after overnight curing at 100^{o}C in a convection oven. 20G stainless steel tubes with a length of 1.5cm (Coopers Needle Works, UK) were carefully bent to 90^{o} angles using pliers, inserted into access ports and secured using two-part epoxy glue (Araldite, USA).

Cell culture

HPAECs (PromoCell, Cat. No. C-12241) from 3-4 different biological donors were cultured in T75 tissue culture flasks (Sarstedt, Germany, Cat. No. 833911002) coated with 10µg/ml Fibronectin (10 µl/ml, EMD Millipore Corp, USA; 341631) in endothelial cell growth medium 2 (ECGM-2, Promocell, Germany C-22211), supplemented with 2% Foetal Calf Serum (FCS) and growth factor mixes (PromoCell, Cat. No. C-22111): Epidermal Growth Factor (EGF, 5ng/ml), Basic Fibroblast Growth Factor (FGF, 10ng/ml), Insulin-like Growth Factor (IGF, 20ng/L), Vascular Endothelial Growth Factor (VEGF, 0.5ng/ml), Ascorbic Acid (1µg/ml), Heparin (22.5µg/ml), Hydrocortisone (0.2µg/ml); 1% Streptomycin/Penicillin (100µg/ml, Gibco; Cat. No. 15140-122), and 1% MycoZap™ (Lonza, Cat. No. VZA-2032).

HPASMCs (Lonza, Cat. No. CC-2581) were cultured in T75 tissue culture flasks coated with 0.2% porcine gelatin (Sigma, Cat.No. G1890) in smooth muscle cell growth medium 2 (SmGM-2, PromoCell, Cat. No. C-22062), supplemented with 5% FBS and growth factor supplement (PromoCell, Cat. No. C-39267)

containing EGF (0.5ng/ml), Basic FGF (2ng/ml), insulin (5µg/ml), 1% Streptomycin/Penicillin (100µg/mL) and 1% MycoZap™.

For HPAEC and HPASMC co-culture, ECGM-2 medium was supplemented with 10% Foetal Bovine Serum (FBS), 2.5ng/ml epidermal growth factor, 10ng/ml fibroblast growth factor, 20ng/ml insulin like growth factor, 0.5ng/ml vascular endothelial growth factor, 1% Streptomycin/Penicillin (100µg/mL) and 1% MycoZap™, was used. VEGF, Ascorbic Acid, Heparin and Hydrocortisone inhibit HPASMC proliferation and therefore were not added to the media.

To induce hypoxia, cells were incubated in a humidified 37°C incubator set at 5% CO_2, 2% O_2. All cells were used before the sixth passage upon receipt from commercial suppliers.Culture media were sterile filtered using a SteriCup filter unit (Merck, USA, Cat no: SCGPU05RE) prior to use.

Blood-derived human endothelial cells.

Human endothelial colony forming cells (ECFCs) were derived from peripheral blood samples and characterised, as previously described[74]. Venous blood samples were obtained with local ethics committee approval and informed written consent (REC Ref 17/LO/0563) from healthy volunteers (n=5) and HPAH patients with rare pathogenic *BMPR2* variants (n=5). ECFCs were cultured in 1% porcine gelatin- coated T75 tissue culture flasks (Sigma, Cat.No. G1890) in EGM-2 medium (CC-3156, Lonza Biologics, Slough, UK), supplemented with growth factors (CC-4176, EGMTM-2 bullet kit, Lonza), 20% FBS (HyClone, Thermo Scientific, South Logan, UT, USA) and 1% antibiotic/antimycotic solution (Gibco, Invitrogen, Paisley, UK). All ECFCs were used between passages 3-6.

Demographic and clinical features of healthy subjects and PAH patients are shown in Supplementary Table S2 and IPAH *BMPR2* mutation variants are listed in Supplementary Table S3.

HPAEC and HPASMC co-culture in Transwell filters

12mm Transwell inserts containing a polyethylene terephthalate (PET) membrane with 0.4µm pores and a pore density of (2.0 ± 0.4) X 10 pores per cm² (Cat no: 353180, Corning, USA) were coated with sterile-filtered 100µg/ml rat tail collagen (BD Biosciences, UK; Cat: 354236) in 20mM acetic acid (Honeywell, UK; Cat no: 695092) for 1 hour at room temperature. First, the Transwell inserts were inverted, with the bottom part of the filter facing up and 125,000 HPASMCs suspended in 100µl of co-culture medium were seeded onto the surface of the filter. After 1 hour, the unattached cells were gently removed with PBS and the inserts were placed in the wells of a 12-well plate filled with 0.5mL co-culture medium, with HPASMCs facing down. Then, 125,000 HPAECs suspended in 0.3mL of co-culture medium were plated inside the insert, to create a direct endothelial-smooth muscle cell co-culture on both sides of the PET membrane. Culture media in the top and bottom compartment of the Transwell dish were changed every 48 hours. Cells were used for experiments 2 days post-confluence.

On-Chip cell co-culture

Microfluidic channels were sterilised during manufacture using oxygen plasma and additionally sterilised under UV light for 30 minutes. Inlets/outlets of channels not used in this procedure, were covered with 3M Magic Tape. Chips selected for use were flushed with 100% ethanol, followed by two washes with sterile PBS. Before seeding cells, microfluidic channels were filled with sterile 100µg/ml rat tail collagen (BD Biosciences, UK; Cat: 354236) in 20mM acetic acid (Honeywell, UK; Cat: 695092) and incubated for 1 hour at room temperature. Following coating, 150,000 HPASMCs suspended in 15µl of co-culture medium were seeded into the smooth muscle (bottom) channel. The chip was turned over and placed in a humidified 37°C incubator for 2 hours to allow cell attachment. The smooth muscle chamber was then gently flushed with co-culture medium to remove unattached cells and the chip was reverted to the upright position. 150,000 HPAEC or ECFCs suspended in 15µl (10,000 cells/µl) of co-culture medium were seeded into the endothelial (top) channel and incubated for 2 hours at 37°C. The endothelial cell and smooth muscle cell channels were then gently flushed with 200µl co-culture media to remove non-adherent cells, before connecting access ports to custom media reservoirs (Cambridge Glassblowing, UK) via 0.8mm ID flexible tubing (IBIDI, Germany, cat: 10841). Medium was perfused using a REGLO ICC 4 channel 12 Roller Pump (Cole-Parmer, UK, cat: ISM4412), utilising Ismatec Pump Tubing, PharMed® BPT, 0.76 mm ID; 100 ft (Cole-Parmer, UK, cat: WZ-95809-24) and Ismatec Pump Tubing, 3-Stop, PharMed® BPT, 0.76 mm ID (Cole-Parmer, UK, cat: WZ-95714-24). 0.8mm ID Y-Style polypropylene barbed flow splitters were used to partition flow between two chips in an independent flow circuit (IBIDI, Germany, cat: 10827). All chips were perfused with 6 dynes/cm^2 flow.

BMPR2 knockdown

~90% confluent HPAECs grown in 6 well plates were infected with Ad-Control-shRNA-GFP (Vector Biolabs, USA; Cat. No: 1122) or Ad-BMPR2-shRNA-GFP (Vector Biolabs, USA; Cat. No: shADV-202207) (titre 1x10^8 PFU/mL) at the multiplicity of infection (MOI) of 1:750. Three hours later, media were changed and cells were incubated for 24-48 hours before further experimentation. Transfection efficiencies were determined by fluorescent cell counting and BMPR2 knockdown was confirmed by qPCR and western blotting.

RNA Isolation

Cultured cells wells were washed in PBS and trypsinised (Cat: 25200072; Gibco, UK) to facilitate cell detachment. Trypsin was neutralised with DMEM containing 10% FBS and the cell suspension was collected in RNase-free LoBind 1.5mL microcentrifuge tubes (Cat: Z666548-250EA; Merck Life Science, UK). Cells were centrifuged for 5 minutes at 5000g at room temperature and residual medium was aspirated without disturbing the cell pellet. Tubes were either stored at -80^{o}C or taken immediately for RNA isolation. Before the RNA isolation, all surfaces and pipettes were treated with RNase-Zap RNase Decontamination Solution (Cat: AM9780; Invitrogen, UK) and sprayed with 70% Ethanol. Total RNA was extracted using either a Monarch Total RNA Miniprep Kit (Cat: T2010S; New England Biolabs, MA, USA) or RNeasy Plus Micro Kit (Cat: 74034; Qiagen, Germany), according to manufacturer's protocols, with the modification of 0.5-fold reduction in the recommended centrifugation speed in all steps except for the final wash and elution in RNase-free water. Double elutions were performed to maximise RNA recovery

from spin columns. Total RNA levels were quantified using a NanoDrop™ ND2000 spectrophotometer (Thermo Scientific, UK). The ratio of absorbance at 260nm and 280nm (A260/A280) was used to evaluate RNA purity, with values above 1.8 considered acceptable quality. RNA was then stored at -80°C for future experiments.

Reverse Transcription

50ng (from chips) or 100ng (from all other samples) of extracted RNA was reverse transcribed into cDNA using a LunaScript RT SuperMix Kit (Cat: E3010L; New England Biolabs, MA, USA). Samples were prepared on ice for RT in PCR-certified 96well plates in a total volume of 20µl. cDNA samples were all diluted with RNase-free water to make a 1ng/µl cDNA solution (30µl or 70µl was added to chip and all other sample cDNAs respectively) and either stored at -20^{o}C or immediately used for qPCR. Components of RT reaction mix and RT cycle are detailed in Supplementary Tables S4 and S5.

qPCR

1µl of 1ng cDNA was used in each individual well for PCR. Master mixes for each gene of interest were created using Luna Universal qPCR Master Mix (Cat: M3003E; New England Biolabs, MA, USA), primers and water, as outlined in Supplementary Table S6. All primer sequences were designed from FASTA sequences (PubMed, NCBI). List of primers is shown in Supplementary Table S7.

RNA sequencing

Next-generation RNA sequencing of HPAECs transfected with Ad-shCTL or Ad-shBMPR2, HPASMCs, healthy volunteer ECFCs and PAH ECFCs with 4-5 biological replicates, was performed at the Imperial British Research Council Genomics Facility (Imperial College London, UK). RNA quality and quantity was determined using a Tapestation System (Agilent Technologies, UK). 50ng of high-quality total RNA (RNA Integrity Number Score ≥8.0) was used as starting material. Polyadenylated mRNA enrichment was performed using a NEBNext® Poly(A) mRNA Magnetic Isolation Module (Cat: E7490L; New England Biolabs, MA, USA). RNA libraries were prepared using a NEBNext® Ultra™ II Directional RNA Library Prep Kit (Cat: E7760L; New England Biolabs, MA, USA), in accordance with the manufacturer's protocol. Samples were indexed at the PCR enrichment stage of RNA library preparation with NEBNext Multiplex Oligos for Illumina 96 Unique Dual Index Primer Pairs (Cat: E6440L; New England Biolabs, MA, USA). RNA sequencing was then performed on an Illumina Hiseq4000 Paired End 75 with dual indexing (Illumina, CA, USA) yielding ~25-30 million reads per sample.

Raw sequencing data (fastq files) were aligned to a reference human transcriptome (GENCODE release 34) using Salmon (v1.4.0)[75] to produce transcript abundance estimates. Estimates were converted to gene expression data in RStudio (https://www.R-project.org/) using the R package tximport. Differential gene expression was performed using edgeR (v3.30.3)[76], which utilises the limma R package (v3.44.3)[77] adapted for optimising performance in selecting differentially expressed genes in relatively low numbers of biological replicates. This analysis was corrected for at least 2 principal components, which each

component individually explaining >1% of variance in the dataset. Genes were considered differentially expressed if the P value was <0.05 and the absolute fold change was >0.25. Functional annotation and enrichment of genes was performed using GSEA software (Broad Institute, MIT; UC San Diego) and Ingenuity Pathway Analysis (IPA, Qiagen) using in-built false discovery rate multiple test corrections. Prior to GSEA analysis, genes that met DGE thresholds were pre-ranked following the guidelines from[78], and were analysed using the following gene set collections from the Molecular Signatures Database (MSigDB): Hallmark[79], KEGG[80] or Reactome[81]. The following R packages were used to produce selected graphs: Volcano plots using EnhancedVolcano (https://github.com/kevinblighe/EnhancedVolcano); dot plots using ggplot2 (https://ggplot2.tidyverse.org); heatmaps using pheatmap (https://cran.r-project.org/package=pheatmap).

Comparative analysis with published RNAseq datasets

RNAseq datasets used for comparative analysis were from HPASMCs isolated from IPAH lung transplants[22] and HPAECs isolated from IPAH lung transplants[23]. Other databases of genes with known PAH associations were downloaded from Supplementary File 4[24] (Disgenet public website https://www.disgenet.org/search; DisGENET PAH (https://www.disgenet.org/browser/0/1/0/C2973725/), DisGENET IPAH (https://www.disgenet.org/browser/0/1/0/C3203102/

Permeability assays

Transwell assay: 500µl medium containing 1mg/ml FITC-Dextran[74] was added to the apical compartment of the transwell insert and was incubated for 1 hour. 1ml from the lower compartment was collected after one hour and fluorescence of FITC-dextran was measured in a GLOMAX spectrophotometer (Promega, USA) at excitation/emission 490/525nm. For thrombin-based experiments, 1U/ml thrombin (T7513, Sigma Aldrich, Dorset, UK) was added to the co-culture media containing 1mg/ml FITC-Dextran and the experiment was performed as described above.

Microfluidic permeability assay: 1mg/ml 40kDa FITC-Dextran (FD40S, Sigma Aldrich, Dorset, UK) was added to co-culture medium and perfused through the top channel at 6 dynes/cm^2. Perfusion was stopped after one hour and the lower smooth muscle cell channel was gently flushed with 250µl of medium and collected for analysis on a GLOMAX spectrophotometer (Promega, USA) at excitation/emission 490/525nm.

Apparent permeability Papp [cm/s] was determined using the formula[82]:

$$P_{app} = V_r \cdot C_r \,/\, [A \cdot t \cdot (C_{d\text{-}out} \cdot V_d + C_r \cdot V_r) \,/\, (V_d + V_r)]$$

Where:

- V_r is volume of receiving channel at time *t*
- V_d is volume of dosing channel at time *t*;

- A is area of membrane, which for our system is 0.1433333cm^2
- C_r is measured concentration of tracer in the receiving channel
- $C_{d\text{-}out}$ is measured concentration of tracer in the dosing channel effluent

Immunostaining

Cells were fixed in 4% paraformaldehyde (Sigma Aldrich, UK) (w/v) in PBS for 20 minutes, washed 3 x in PBS and permeabilised in 0.1% Triton-X-100 (Sigma Aldrich, UK) (v/v) in PBS for 5 minutes. Samples were then incubated in blocking buffer containing: 0.1% Triton-X-100 (Sigma Aldrich, UK) (v/v) with either 5% Normal Goat Serum (NGS; Cat: 31873, Invitrogen, UK) or 2% BSA (A9418, Sigma Aldrich, UK) in PBS for 30mins. Primary antibodies were added at appropriate dilutions in a solution containing 2.5% NGS and 0.05% Triton-X-100 (v/v) in PBS for 2 hours at room temperature or left overnight at 4^{o}C. Samples were washed 3x in PBS and secondary antibodies were incubated accordingly for 1 hour. Samples were washed 3x in PBS and were mounted in VECTASHIELD® Antifade Mounting Medium with DAPI (Vector Laboratories, UK, Cat: H-1200). A list of primary and secondary antibodies used is shown in **Supplementary Table S8**. Immunostained samples were visualised under a Zeiss LSM-780 inverted confocal laser scanning microscope (Carl Zeiss AG, Germany) or a fluorescent Zeiss AxioObserver widefield microscope (Carl Zeiss AG, Germany) with x5, x10 or x20 objective.

istological sections of lung tissues from treatment-naïve PAH patients at lung transplantation (n=2), and control tissues comprising uninvolved regions of lobectomy specimens from 2 unused donor lungs were from the tissue archives at Hammersmith Hospital, Imperial College London. Tissue samples were fixed in 10% formaldehyde in PBS and embedded in wax, and sections were processed for immunohistochemistry as previously described[83]. Briefly, dewaxed and deparaffinised tissue sections were blocked for 1 hour at room temperature with 3% normal horse serum (Vector Laboratories) in 1X PBS containing 0.1% bovine serum albumin (Sigma-Aldrich) and 0.01% sodium azide (Sigma-Aldrich) and then incubated with anti- von Willebrand Factor antibody (to label endothelium) and anti- smooth muscle actin antibody (to label smooth muscle cells) at 4°C overnight. After 3x washes in PBS, slides were incubated with secondary, fluorescently-labelled anti-rabbit and anti-mouse antibodies for 30 minutes at room temperature. Following immunostaining, tissues were mounted in VECTASHIELD® Antifade Mounting Medium with DAPI (Vector Laboratories, UK, Cat: H-1200) and examined under a fluorescent confocal microscope (Leica, TCS SP5, Leica Biosystems, Bretton, Peterborough).

List of primary and secondary antibodies used for immunostaining is provided in **Supplementary Table S8**.

EdU Proliferation Assay

Cell proliferation was quantified using an EdU Cell Proliferation Assay Kit (EdU-594, EMD Millipore Corp, USA, Cat. No. 17-10527). EdU nucleotides were added directly to cell culture medium at a dilution of 1:1000, 24 hours before the end of experiment. Cells were fixed, permeabilized and blocked as in

immunostaining method, and were treated with the assay reaction cocktail, prepared according to the manufacturer's instructions. EdU positive cells were visualized under a fluorescent Zeiss AxioObserver widefield microscope (Carl Zeiss AG, Germany). Images and z-stacks were taken with x10 objective and were analysed with ImageJ software. Data is presented as a percentage of the number of EdU positive cells vs the total cell number.

Imatinib treatment

Imatinib Mesylate (Enzo life sciences, UK; Cat: ALX-270-492-M025) was added directly to cell culture medium at a 10μM concentration[84]. Experiments were conducted for 24 hours under normoxic (21% O_2) or hypoxic (2% O_2) conditions accordingly.

Apoptosis assay

Apoptosis was measured using a Click-iT Plus TUNEL Assay for In Situ Apoptosis Detection Kit with Alexa Fluor 647 dye (Life Technologies, Cat: C10619), as per the manufacturer's instructions. TUNEL positive cells were visualized under a fluorescent Zeiss AxioObserver widefield microscope (Carl Zeiss AG, Germany). Images and z-stacks were taken under x10 objective and analysed with ImageJ software. Data is presented as a percentage of the number of TUNEL positive cells vs total cell number.

Cell counting

3D Z-stacks of tiled, 5μm-thick image slices of microfluidic channels were acquired under AxioObserver widefield microscope. In microfluidic channels, endothelial cells (HPAECs or ECFCs) were labelled green (GFP), nuclei of proliferating cells (HPAEC/ECFCs and HPASMC) were labelled red (EdU-647) and nuclei of all cells were labelled blue (DAPI). Image stacks were flattened and three 500μm x 1000μm regions of interest were selected at the front, middle and at the end of each channel, within the area of HPAEC/HPASMC overlap. To facilitate cell counting, a custom ImageJ script was developed that generated a binary black/white mask of fluorescent signatures (cells and nuclei) within each colour channel. Green cells with blue nuclei were classed as quiescent ECs, green cells with blue/red nuclei were classed as proliferating ECs and the remaining cells (not green) with blue nuclei only and blue/red nuclei only, were classed as quiescent SMCs and proliferating SMCs, respectively. Counts were made within each colour channel before overlaying images with DAPI binary mask to produce final counts. Selected counts were additionally checked by manual scoring of cells in each fluorescent channel using the "Grid" and "CellCounter" plugins in ImageJ.

Analysis of cell shape and alignment

ImageJ analysis software was used to measure cell alignment and cell elongation. Alignment was determined as the angle between the long axis of the cell and the horizontal axis of the image at 180^o and values were expressed as the percentage of cells at a particular angle of orientation; Elongation was determined as 1-circularity [long axis/short axis of the cell].

Western blotting

Cells were washed 3x in ice-cold PBS and lysed using RIPA buffer (Sigma, UK) containing 1x proteinase and phosphatase inhibitor cocktail (ThermoFisher, UK; cat no: 78440). Protein concentration in samples was measured using a Pierce™ BCA Protein Assay Kit (Thermo Fisher Scientific, UK, 23225) using standard protocols and absorbance was measured in a GLOMAX spectrophotometer (Glomax™ luminometer; Promega, USA). Samples were resolved with 4x Laemmli SDS reducing sample buffer (Alfa Aesar, MA, USA; Cat No: J60015) and heated at 95^{o}C for 10 minutes. 10-20µg of protein per sample was loaded onto either 10% Mini-PROTEAN® TGX™ Precast Protein Gels (10-well, 50µl; Cat No: #4561034; Bio-Rad, CA, USA) or a pre-cast 4-12% bis-tris Nu-PAGE gel (Invitrogen, UK). 5µl of Spectra Multicolour Broad Range Protein Ladder (ThermoFisher, UK; cat no: 26634) was loaded into the first well of each gel in order to estimate protein molecular weights within samples during blot imaging. Samples were separated by SDS-PAGE in NuPAGE™ MES (2-(N-morpholino)ethanesulfonic acid; Cat: NP0002; Invitrogen, UK) or NuPAGE™ MOPS (3-(N-morpholino)propanesulfonic acid; Cat: NP0001; Invitrogen, UK) buffer at 200V for 35 minutes. Proteins were transferred onto PVDF or nitrocellulose membranes using a trans-blot turbo transfer system (Biorad, UK). Membranes were blocked in freshly prepared 5% Semi-skimmed milk (Cat: 70166-500G; Merck, UK) or 5% (w/v) bovine serum albumin (BSA) (Cat: A9418; Sigma, UK) in TBST (2.42g Tris, 8g Sodium Chloride, 1L double distilled Millipore water, 1ml Tween-20, adjusted to pH 7.8) for one hour and then incubated overnight at 4^{o}C with the appropriate primary antibody. After that, membranes were washed 5x for 3 minutes each with fresh TBST and incubated with appropriate HRP-conjugated secondary antibodies in TBST for one hour and then washed 3x 15 minutes in TBST. Bands were visualised using Crescendo ECL detection reagent (Merck-Millipore, USA) with a ChemiDoc MP Imaging System (Biorad, UK). Primary and secondary antibodies used for western blotting are listed in **Supplementary Table S9**. Band intensity was determined by densitometry using ImageJ software. Expression of proteins of interest was normalised to b-actin.

Statistical analysis and data presentation

All graphs were either plotted in RStudio or Graphpad Prizm 8 software (Graphpad Software Inc, CA, USA), with statistical tests performed, as appropriate. In bar graphs, error bars indicate the standard error of the mean (SEM). When comparing two sample groups, normally distributed data was analysed using an unpaired student's t test. For comparisons of two or more sample groups, one or two way ANOVA was used, as appropriate. The threshold for statistical significance was $P < 0.05$.

Declarations

Study approval

Venous blood samples were obtained with local ethics committee approval and informed written consent from healthy volunteers and idiopathic PAH patients. Participants were identified by number. ethics committee approval and informed written consent (REC Ref 17/LO/0563)

Data availability.

All data generated or analysed during this study are included in this published article (and its supplementary information files) are available from the corresponding author upon reasonable request. Gene datasets will be made available upon the acceptance of the manuscript.

AUTHOR CONTRIBUTIONS. AJA performed chip fabrication, designed and performed experiments, analysed data and wrote the manuscript; TS performed *in silico* computational simulations, wrote the manuscript; CJR provided code and assisted with performing RNAseq analysis and critically evaluated the manuscript; SS and AF performed qPCRs; MRW, JW & LSH provided patient material and critically evaluated the manuscript ; JBE provided guidance on *in silico* simulations, chip design and fabricationnd critically evaluated the manuscript. BWS conceived the study, designed experiments, secured funding and wrote the manuscript.

ACKNOWLEDGEMENTS

This research was supported by the BHF PhD Studentship FS/17/64/33476 (Alex Ainscough), British Heart Foundation project grant PG/19/19/34286, BHF Imperial Centre of Research Excellence grant RE/18/4/34215 and ICIC (MRC) Confidence in Concept 20/21 grant 4050789012. JBE has been supported by the European Research Council (ERC) under the European Union's Horizon 2020 research and innovation program (grant agreement No 724300 and 875525).

We thank the staff of the NIHR Imperial Clinical Research Facility, Hammersmith Hospital (London UK), Mr. Lee Tooley of the Imperial College Mechanical Instrumentation Workshop for his help in fabricating the racks and trays for the flow system, Mr. Joshua Dodd (Morgan Branding) for help in preparation of scientific illustrations, Dr Hebah Sindi (Imperial College London) for help with immunostaining of human lung sections and Dr Sandro Satta (Imperial College London) for help with optimising RNA extractions and qPCR. We are particularly grateful to Mr Steve Rothery (Imperial FILM facility) for his help and advice with image acquisition and analysis. All widefield/confocal imaging analysis was performed at the Facility for Imaging by Light Microscopy (FILM) at Imperial College London, which is part-supported by funding from the Wellcome Trust (grant 104931/Z/14/Z) and BBSRC (grant BB/L015129/1).

References

1 Hoeper, M. M. *et al.* A global view of pulmonary hypertension. *Lancet Respir Med* **4**, 306-322, doi:10.1016/S2213-2600(15)00543-3 (2016).

2 Sakao, S., Tatsumi, K. & Voelkel, N. F. Endothelial cells and pulmonary arterial hypertension: apoptosis, proliferation, interaction and transdifferentiation. *Respir Res* **10**, 95, doi:10.1186/1465-9921-10-95 (2009).

3 Humbert, M. *et al.* Pathology and pathobiology of pulmonary hypertension: state of the art and research perspectives. *Eur Respir J* **53**, doi:10.1183/13993003.01887-2018 (2019).

4 Dannewitz Prosseda, S., Ali, M. K. & Spiekerkoetter, E. Novel Advances in Modifying BMPR2 Signaling in PAH. *Genes (Basel)* **12**, doi:10.3390/genes12010008 (2020).

5 Yuan, J. X. & Rubin, L. J. Pathogenesis of pulmonary arterial hypertension: the need for multiple hits. *Circulation* **111**, 534-538, doi:10.1161/01.CIR.0000156326.48823.55 (2005).

6 Southgate, L., Machado, R. D., Graf, S. & Morrell, N. W. Molecular genetic framework underlying pulmonary arterial hypertension. *Nat Rev Cardiol* **17**, 85-95, doi:10.1038/s41569-019-0242-x (2020).

7 Long, L. *et al.* Chloroquine prevents progression of experimental pulmonary hypertension via inhibition of autophagy and lysosomal bone morphogenetic protein type II receptor degradation. *Circ Res* **112**, 1159-1170, doi:10.1161/CIRCRESAHA.111.300483 (2013).

8 Rai, N., Shihan, M., Seeger, W., Schermuly, R. T. & Novoyatleva, T. Genetic Delivery and Gene Therapy in Pulmonary Hypertension. *Int J Mol Sci* **22**, doi:10.3390/ijms22031179 (2021).

9 Carman, B. L., Predescu, D. N., Machado, R. & Predescu, S. A. Plexiform Arteriopathy in Rodent Models of Pulmonary Arterial Hypertension. *Am J Pathol* **189**, 1133-1144, doi:10.1016/j.ajpath.2019.02.005 (2019).

10 Hoeper, M. M. *et al.* Imatinib mesylate as add-on therapy for pulmonary arterial hypertension: results of the randomized IMPRES study. *Circulation* **127**, 1128-1138, doi:10.1161/CIRCULATIONAHA.112.000765 (2013).

11 Aiello, V. D. *et al.* Morphology of the internal elastic lamina in arteries from pulmonary hypertensive patients: a confocal laser microscopy study. *Mod Pathol* **16**, 411-416, doi:10.1097/01.MP.0000067685.57858.D7 (2003).

12 Gairhe, S., Bauer, N. N., Gebb, S. A. & McMurtry, I. F. Myoendothelial gap junctional signaling induces differentiation of pulmonary arterial smooth muscle cells. *Am J Physiol Lung Cell Mol Physiol* **301**, L527-535, doi:10.1152/ajplung.00091.2011 (2011).

13 Truong, U. *et al.* Wall shear stress measured by phase contrast cardiovascular magnetic resonance in children and adolescents with pulmonary arterial hypertension. *J Cardiovasc Magn Reson* **15**, 81, doi:10.1186/1532-429X-15-81 (2013).

14 Huh, D. *et al.* Reconstituting organ-level lung functions on a chip. *Science* **328**, 1662-1668, doi:10.1126/science.1188302 (2010).

15 Draijer, R., Atsma, D. E., van der Laarse, A. & van Hinsbergh, V. W. cGMP and nitric oxide modulate thrombin-induced endothelial permeability. Regulation via different pathways in human aortic and

umbilical vein endothelial cells. *Circ Res* **76**, 199-208, doi:10.1161/01.res.76.2.199 (1995).

16 Bogatcheva, N. V., Garcia, J. G. & Verin, A. D. Molecular mechanisms of thrombin-induced endothelial cell permeability. *Biochemistry (Mosc)* **67**, 75-84, doi:10.1023/a:1013904231324 (2002).

17 Sakolish, C. M., Esch, M. B., Hickman, J. J., Shuler, M. L. & Mahler, G. J. Modeling Barrier Tissues In Vitro: Methods, Achievements, and Challenges. *EBioMedicine* **5**, 30-39, doi:10.1016/j.ebiom.2016.02.023 (2016).

18 Burton, V. J. *et al.* Bone morphogenetic protein receptor II regulates pulmonary artery endothelial cell barrier function. *Blood* **117**, 333-341, doi:10.1182/blood-2010-05-285973 (2011).

19 Abdul-Salam, V. B. *et al.* Chloride intracellular channel protein 4 in pulmonary endothelial angiogenesis. *Vasc Pharmacol* **56**, 361-361, doi:10.1016/j.vph.2011.08.152 (2012).

20 Sindi, H. A. *et al.* Therapeutic potential of KLF2-induced exosomal microRNAs in pulmonary hypertension. *Nat Commun* **11**, 1185, doi:10.1038/s41467-020-14966-x (2020).

21 Smits, J. *et al.* Blood Outgrowth and Proliferation of Endothelial Colony Forming Cells are Related to Markers of Disease Severity in Patients with Pulmonary Arterial Hypertension. *Int J Mol Sci* **19**, doi:10.3390/ijms19123763 (2018).

22 Gorr, M. W., Sriram, K., Muthusamy, A. & Insel, P. A. Transcriptomic analysis of pulmonary artery smooth muscle cells identifies new potential therapeutic targets for idiopathic pulmonary arterial hypertension. *Br J Pharmacol* **177**, 3505-3518, doi:10.1111/bph.15074 (2020).

23 Rhodes, C. J. *et al.* RNA Sequencing Analysis Detection of a Novel Pathway of Endothelial Dysfunction in Pulmonary Arterial Hypertension. *Am J Respir Crit Care Med* **192**, 356-366, doi:10.1164/rccm.201408-1528OC (2015).

24 Reyes-Palomares, A. *et al.* Remodeling of active endothelial enhancers is associated with aberrant gene-regulatory networks in pulmonary arterial hypertension. *Nat Commun* **11**, 1673, doi:10.1038/s41467-020-15463-x (2020).

25 Gorr, M. W., Sriram, K., Chinn, A. M., Muthusamy, A. & Insel, P. A. Transcriptomic profiles reveal differences between the right and left ventricle in normoxia and hypoxia. *Physiol Rep* **8**, e14344, doi:10.14814/phy2.14344 (2020).

26 Shi, Z. D. & Tarbell, J. M. Fluid flow mechanotransduction in vascular smooth muscle cells and fibroblasts. *Ann Biomed Eng* **39**, 1608-1619, doi:10.1007/s10439-011-0309-2 (2011).

27 van Engeland, N. C. A. *et al.* A biomimetic microfluidic model to study signalling between endothelial and vascular smooth muscle cells under hemodynamic conditions. *Lab Chip* **18**, 1607-1620, doi:10.1039/c8lc00286j (2018).

28 Xiao, Y. *et al.* Pathological Mechanisms and Potential Therapeutic Targets of Pulmonary Arterial Hypertension: A Review. *Aging Dis* **11**, 1623-1639, doi:10.14336/AD.2020.0111 (2020).

29 Lebrin, F., Deckers, M., Bertolino, P. & Ten Dijke, P. TGF-beta receptor function in the endothelium. *Cardiovasc Res* **65**, 599-608, doi:10.1016/j.cardiores.2004.10.036 (2005).

30 Morty, R. E. *et al.* Dysregulated bone morphogenetic protein signaling in monocrotaline-induced pulmonary arterial hypertension. *Arterioscler Thromb Vasc Biol* **27**, 1072-1078, doi:10.1161/ATVBAHA.107.141200 (2007).

31 Maloney, J. P. *et al.* Loss-of-function thrombospondin-1 mutations in familial pulmonary hypertension. *Am J Physiol Lung Cell Mol Physiol* **302**, L541-554, doi:10.1152/ajplung.00282.2011 (2012).

32 Lowery, J. W. *et al.* ID family protein expression and regulation in hypoxic pulmonary hypertension. *Am J Physiol Regul Integr Comp Physiol* **299**, R1463-1477, doi:10.1152/ajpregu.00866.2009 (2010).

33 Zhang, Y. *et al.* E3 Ubiquitin ligase NEDD4 familyregulatory network in cardiovascular disease. *Int J Biol Sci* **16**, 2727-2740, doi:10.7150/ijbs.48437 (2020).

34 Hiepen, C. *et al.* BMPR2 acts as a gatekeeper to protect endothelial cells from increased TGFbeta responses and altered cell mechanics. *PLoS Biol* **17**, e3000557, doi:10.1371/journal.pbio.3000557 (2019).

35 Zweier, J. L. & Talukder, M. A. Targeting dimethylarginine dimethylaminohydrolases in pulmonary arterial hypertension: a new approach to improve vascular dysfunction? *Circulation* **123**, 1156-1158, doi:10.1161/CIRCULATIONAHA.110.017038 (2011).

36 Leiper, J. *et al.* Disruption of methylarginine metabolism impairs vascular homeostasis. *Nat Med* **13**, 198-203, doi:10.1038/nm1543 (2007).

37 Rhodes, C. J. *et al.* Genetic determinants of risk in pulmonary arterial hypertension: international genome-wide association studies and meta-analysis. *Lancet Respir Med* **7**, 227-238, doi:10.1016/S2213-2600(18)30409-0 (2019).

38 Gross, C. M. *et al.* Sox18 preserves the pulmonary endothelial barrier under conditions of increased shear stress. *J Cell Physiol* **229**, 1802-1816, doi:10.1002/jcp.24633 (2014).

39 Eichstaedt, C. A. *et al.* First identification of Kruppel-like factor 2 mutation in heritable pulmonary arterial hypertension. *Clin Sci (Lond)* **131**, 689-698, doi:10.1042/CS20160930 (2017).

40 Eyries, M. *et al.* Familial pulmonary arterial hypertension by KDR heterozygous loss of function. *Eur Respir J* **55**, doi:10.1183/13993003.02165-2019 (2020).

41 Jasmin, J. F. *et al.* Lung remodeling and pulmonary hypertension after myocardial infarction: pathogenic role of reduced caveolin expression. *Cardiovasc Res* **63**, 747-755, doi:10.1016/j.cardiores.2004.05.018 (2004).

42 Yeo, Y. *et al.* FGF12 (Fibroblast Growth Factor 12) Inhibits Vascular Smooth Muscle Cell Remodeling in Pulmonary Arterial Hypertension. *Hypertension* **76**, 1778-1786, doi:10.1161/HYPERTENSIONAHA.120.15068 (2020).

43 Wojciak-Stothard, B. *et al.* Role of RhoB in the regulation of pulmonary endothelial and smooth muscle cell responses to hypoxia. *Circ Res* **110**, 1423-1434, doi:10.1161/CIRCRESAHA.112.264473 (2012).

44 Sevilla-Perez, J. *et al.* Shroom expression is attenuated in pulmonary arterial hypertension. *Eur Respir J* **32**, 871-880, doi:10.1183/09031936.00045507 (2008).

45 Ma, L. *et al.* A novel channelopathy in pulmonary arterial hypertension. *N Engl J Med* **369**, 351-361, doi:10.1056/NEJMoa1211097 (2013).

46 Cunningham, K. P. *et al.* Characterization and regulation of wild-type and mutant TASK-1 two pore domain potassium channels indicated in pulmonary arterial hypertension. *J Physiol* **597**, 1087-1101, doi:10.1113/JP277275 (2019).

47 Zhao, L. *et al.* Histone deacetylation inhibition in pulmonary hypertension: therapeutic potential of valproic acid and suberoylanilide hydroxamic acid. *Circulation* **126**, 455-467, doi:10.1161/CIRCULATIONAHA.112.103176 (2012).

48 Van der Feen, D. E. *et al.* Multicenter Preclinical Validation of BET Inhibition for the Treatment of Pulmonary Arterial Hypertension. *Am J Respir Crit Care Med* **200**, 910-920, doi:10.1164/rccm.201812-2275OC (2019).

49 Backs, J., Song, K., Bezprozvannaya, S., Chang, S. & Olson, E. N. CaM kinase II selectively signals to histone deacetylase 4 during cardiomyocyte hypertrophy. *J Clin Invest* **116**, 1853-1864, doi:10.1172/JCI27438 (2006).

50 Bull, T. M. *et al.* Gene microarray analysis of peripheral blood cells in pulmonary arterial hypertension. *Am J Respir Crit Care Med* **170**, 911-919, doi:10.1164/rccm.200312-1686OC (2004).

51 Kuebler, W. M., Bonnet, S. & Tabuchi, A. Inflammation and autoimmunity in pulmonary hypertension: is there a role for endothelial adhesion molecules? (2017 Grover Conference Series). *Pulm Circ* **8**, 2045893218757596, doi:10.1177/2045893218757596 (2018).

52 Karnik, S. K. *et al.* A critical role for elastin signaling in vascular morphogenesis and disease. *Development* **130**, 411-423, doi:10.1242/dev.00223 (2003).

53 Imanaka-Yoshida, K., Yoshida, T. & Miyagawa-Tomita, S. Tenascin-C in development and disease of blood vessels. *Anat Rec (Hoboken)* **297**, 1747-1757, doi:10.1002/ar.22985 (2014).

54 Mathew, R. Pathogenesis of pulmonary hypertension: a case for caveolin-1 and cell membrane integrity. *Am J Physiol Heart Circ Physiol* **306**, H15-25, doi:10.1152/ajpheart.00266.2013 (2014).

55 Andersen, C. U., Hilberg, O., Mellemkjaer, S., Nielsen-Kudsk, J. E. & Simonsen, U. Apelin and pulmonary hypertension. *Pulm Circ* **1**, 334-346, doi:10.4103/2045-8932.87299 (2011).

56 Hendrickson, R. J. *et al.* Sustained pulsatile flow regulates endothelial nitric oxide synthase and cyclooxygenase expression in co-cultured vascular endothelial and smooth muscle cells. *J Mol Cell Cardiol* **31**, 619-629, doi:10.1006/jmcc.1998.0898 (1999).

57 Zhang, S. *et al.* Bone morphogenetic proteins induce apoptosis in human pulmonary vascular smooth muscle cells. *Am J Physiol Lung Cell Mol Physiol* **285**, L740-754, doi:10.1152/ajplung.00284.2002 (2003).

58 Talati, M. & Hemnes, A. Fatty acid metabolism in pulmonary arterial hypertension: role in right ventricular dysfunction and hypertrophy. *Pulm Circ* **5**, 269-278, doi:10.1086/681227 (2015).

59 Klomp, J. *et al.* Comprehensive transcriptomic profiling reveals SOX7 as an early regulator of angiogenesis in hypoxic human endothelial cells. *J Biol Chem* **295**, 4796-4808, doi:10.1074/jbc.RA119.011822 (2020).

60 Di, R., Yang, Z., Xu, P. & Xu, Y. Silencing PDK1 limits hypoxia-induced pulmonary arterial hypertension in mice via the Akt/p70S6K signaling pathway. *Exp Ther Med* **18**, 699-704, doi:10.3892/etm.2019.7627 (2019).

61 Papandreou, I., Cairns, R. A., Fontana, L., Lim, A. L. & Denko, N. C. HIF-1 mediates adaptation to hypoxia by actively downregulating mitochondrial oxygen consumption. *Cell Metab* **3**, 187-197, doi:10.1016/j.cmet.2006.01.012 (2006).

62 Oishi, Y. & Manabe, I. Kruppel-Like Factors in Metabolic Homeostasis and Cardiometabolic Disease. *Front Cardiovasc Med* **5**, 69, doi:10.3389/fcvm.2018.00069 (2018).

63 Leiherer, A., Geiger, K., Muendlein, A. & Drexel, H. Hypoxia induces a HIF-1alpha dependent signaling cascade to make a complex metabolic switch in SGBS-adipocytes. *Mol Cell Endocrinol* **383**, 21-31, doi:10.1016/j.mce.2013.11.009 (2014).

64 Kawamura, Y., Tanaka, Y., Kawamori, R. & Maeda, S. Overexpression of Kruppel-like factor 7 regulates adipocytokine gene expressions in human adipocytes and inhibits glucose-induced insulin secretion in pancreatic beta-cell line. *Mol Endocrinol* **20**, 844-856, doi:10.1210/me.2005-0138 (2006).

65 Grzegorzewska, A. P. *et al.* Dimethyl Fumarate ameliorates pulmonary arterial hypertension and lung fibrosis by targeting multiple pathways. *Sci Rep* **7**, 41605, doi:10.1038/srep41605 (2017).

66 Jover, E. *et al.* Inhibition of enzymes involved in collagen cross-linking reduces vascular smooth muscle cell calcification. *Faseb J* **32**, 4459-4469, doi:10.1096/fj.201700653R (2018).

67 Sibinga, N. E. *et al.* Collagen VIII is expressed by vascular smooth muscle cells in response to vascular injury. *Circ Res* **80**, 532-541, doi:10.1161/01.res.80.4.532 (1997).

68 Xu, W. *et al.* Integrative proteomics and phosphoproteomics in pulmonary arterial hypertension. *Sci Rep* **9**, 18623, doi:10.1038/s41598-019-55053-6 (2019).

69 Corada, M. *et al.* Sox17 is indispensable for acquisition and maintenance of arterial identity. *Nat Commun* **4**, 2609, doi:10.1038/ncomms3609 (2013).

70 Duong, H. T. *et al.* Pulmonary artery endothelium resident endothelial colony-forming cells in pulmonary arterial hypertension. *Pulm Circ* **1**, 475-486, doi:10.4103/2045-8932.93547 (2011).

71 Al-Hilal, T. A. *et al.* Pulmonary-arterial-hypertension (PAH)-on-a-chip: fabrication, validation and application. *Lab Chip* **20**, 3334-3345, doi:10.1039/d0lc00605j (2020).

72 Toepke, M. W. & Beebe, D. J. PDMS absorption of small molecules and consequences in microfluidic applications. *Lab Chip* **6**, 1484-1486, doi:10.1039/b612140c (2006).

73 Allwardt, V. *et al.* Translational Roadmap for the Organs-on-a-Chip Industry toward Broad Adoption. *Bioengineering (Basel)* **7**, doi:10.3390/bioengineering7030112 (2020).

74 Wojciak-Stothard, B. *et al.* Aberrant chloride intracellular channel 4 expression contributes to endothelial dysfunction in pulmonary arterial hypertension. *Circulation* **129**, 1770-1780, doi:10.1161/CIRCULATIONAHA.113.006797 (2014).

75 Patro, R., Duggal, G., Love, M. I., Irizarry, R. A. & Kingsford, C. Salmon provides fast and bias-aware quantification of transcript expression. *Nat Methods* **14**, 417-419, doi:10.1038/nmeth.4197 (2017).

76 Robinson, M. D., McCarthy, D. J. & Smyth, G. K. edgeR: a Bioconductor package for differential expression analysis of digital gene expression data. *Bioinformatics* **26**, 139-140, doi:10.1093/bioinformatics/btp616 (2010).

77 Ritchie, M. E. *et al.* limma powers differential expression analyses for RNA-sequencing and microarray studies. *Nucleic Acids Res* **43**, e47, doi:10.1093/nar/gkv007 (2015).

78 Reimand, J. *et al.* Pathway enrichment analysis and visualization of omics data using g:Profiler, GSEA, Cytoscape and EnrichmentMap. *Nat Protoc* **14**, 482-517, doi:10.1038/s41596-018-0103-9 (2019).

79 Liberzon, A. *et al.* The Molecular Signatures Database (MSigDB) hallmark gene set collection. *Cell Syst* **1**, 417-425, doi:10.1016/j.cels.2015.12.004 (2015).

80 Kanehisa, M. & Goto, S. KEGG: kyoto encyclopedia of genes and genomes. *Nucleic Acids Res* **28**, 27-30, doi:10.1093/nar/28.1.27 (2000).

81 Fabregat, A. *et al.* Reactome pathway analysis: a high-performance in-memory approach. *BMC Bioinformatics* **18**, 142, doi:10.1186/s12859-017-1559-2 (2017).

82 Maoz, B. M. *et al.* A linked organ-on-chip model of the human neurovascular unit reveals the metabolic coupling of endothelial and neuronal cells. *Nat Biotechnol* **36**, 865-+, doi:10.1038/nbt.4226 (2018).

83 Wojciak-Stothard, B. *et al.* Aberrant Chloride Intracellular Channel 4 Expression Contributes to Endothelial Dysfunction in Pulmonary Arterial Hypertension. *Circulation* **129**, 1770-1780, doi:10.1161/Circulationaha.113.006797 (2014).

84 Aman, J. *et al.* Effective treatment of edema and endothelial barrier dysfunction with imatinib. *Circulation* **126**, 2728-2738, doi:10.1161/CIRCULATIONAHA.112.134304 (2012).

Figures

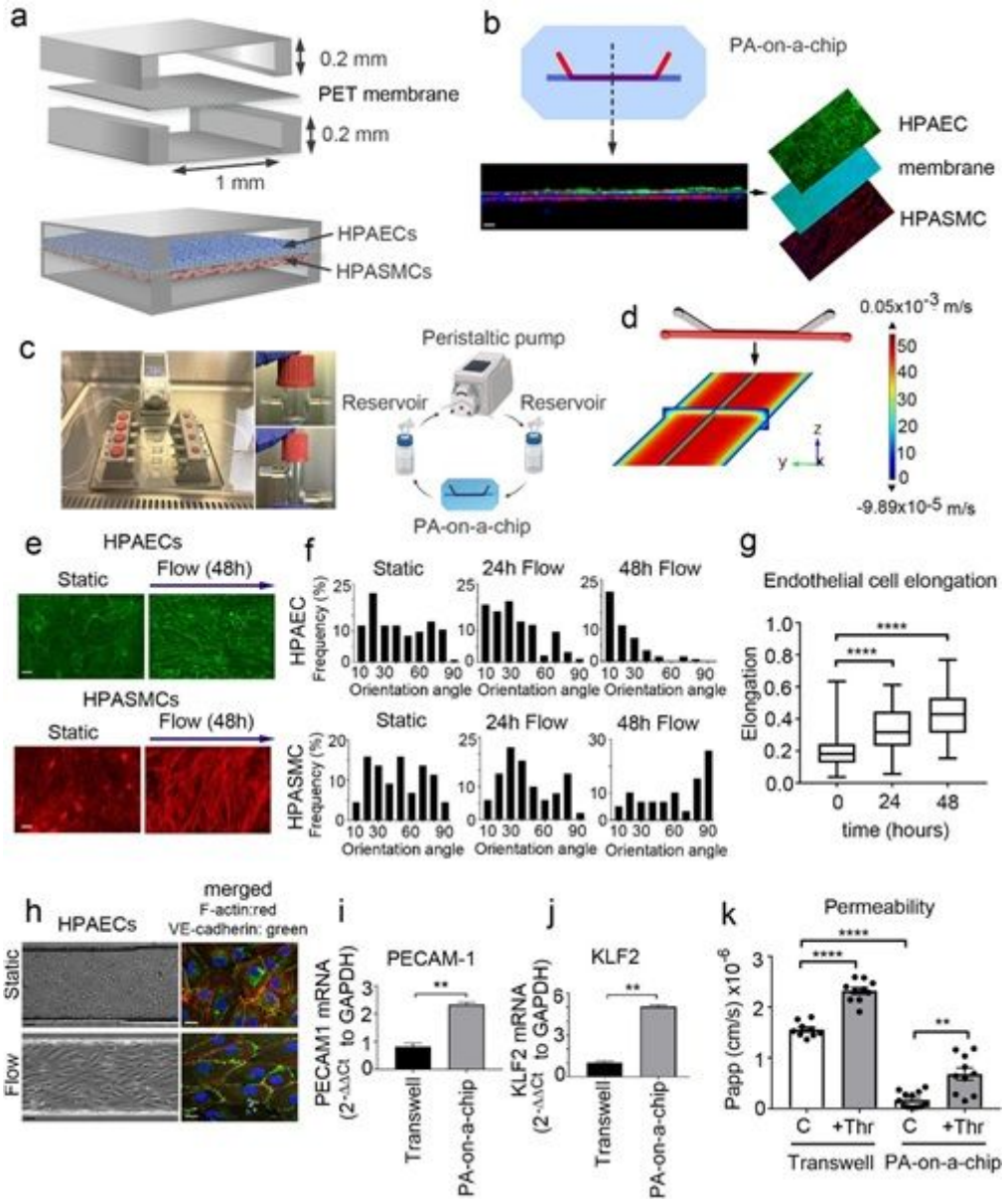

Figure 1

Pulmonary artery-on-a-chip reproduces functionality of a blood vessel. (a) Schematic diagram of the pulmonary artery-on-a-chip (b) Z-section of endothelial-smooth muscle interface, fluorescent confocal imaging. HPAECs (green: VE-cadherin), HPASMCs (red: α-smooth muscle actin). Bar=10μm. (c) Flow system set up comprising peristaltic pump, media reservoirs and chips, perfused with culture medium at 6 dynes/cm2. (d) Fluid-structure interaction (Velocity profile) in endothelial channel, COMSOL modelling. (e) Morphology of HPAECs and HPASMCs under flow, 48h in culture. Confocal microscopy, VE-cadherin: green, α-smooth muscle actin: red. Bar=10μm. (f) Alignment of endothelial and smooth muscle cells at different time points of flow exposure, as indicated. Bar=10μm. (g) Endothelial cell elongation (long axis/short axis of the cell ratio). In (F, G) n=3-4 individual chips per time point. Error bars indicate mean ±SEM of a one-way ANOVA with a Tukey's post-hoc correction test. ****P<0.0001 (h) Phase contract (left) and fluorescent microscopy (right) images of HPAECs grown in microfluidic channels under static and flow conditions, as indicated. F-actin: red, VE-cadherin: green. (i, j) mRNA expression of endothelial

differentiation markers, PECAM-1 and KLF2 in cells treated, as indicated; qPCR. ** = P<0.01; Unpaired t test. n=3. (k) Effects of thrombin (1U/ml) on endothelial barrier function in HPAECs co-cultured with HPASMCs in pulmonary artery-on-a-chip or in transwell dishes. Passage of FITC-dextran (1mg/ml; 1h) from top to bottom channel was used as a measure of endothelial permeability. Cells from 3 different biological donors grown 3-4 chips/transwells per treatment group, were used; n=10-12. Error bars indicate mean ±SEM of a one-way ANOVA with a Tukey's post-hoc correction test. ** P<0.01; ****P<0.0001.

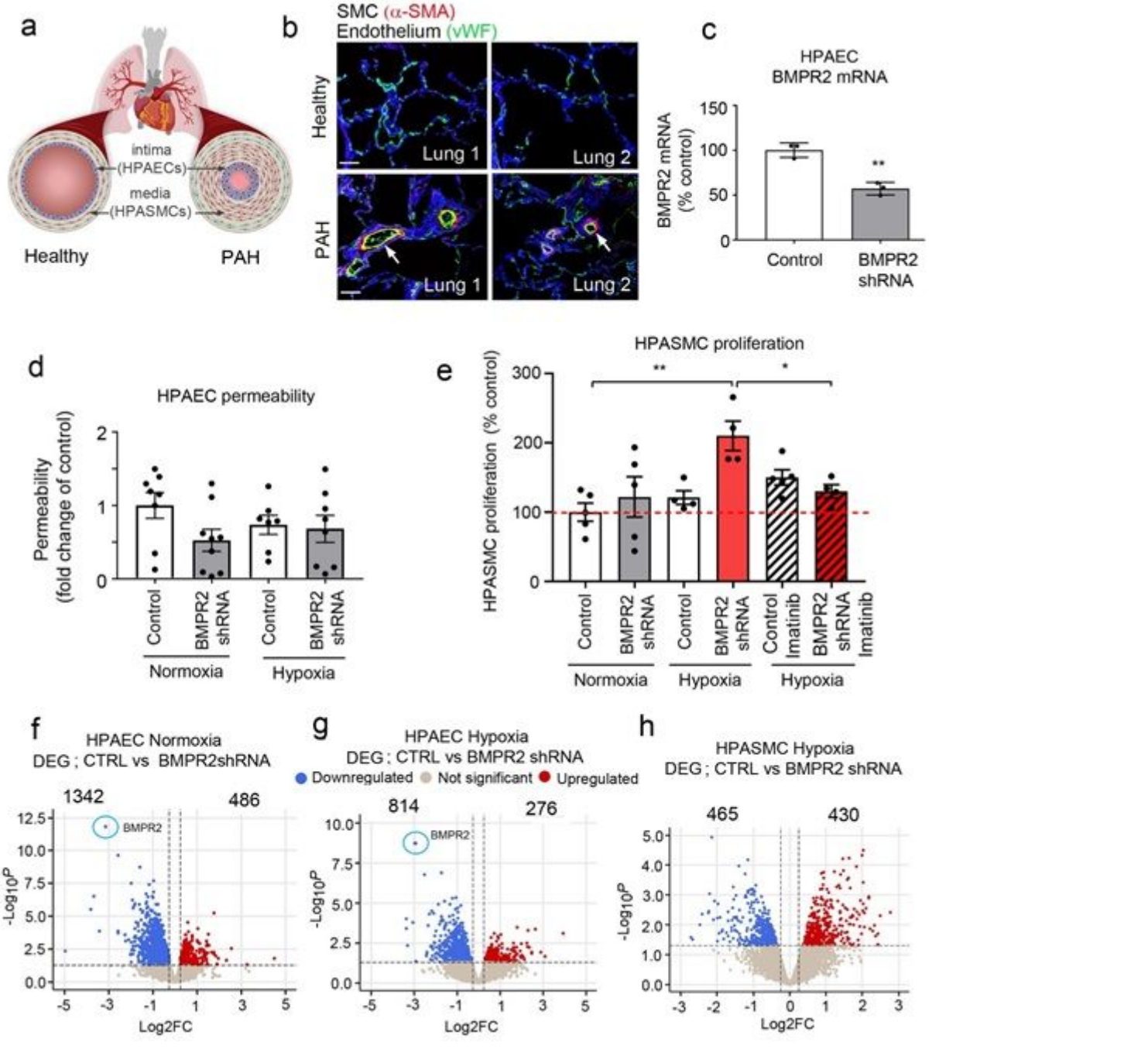

Figure 2

Two-hit model of PAH in pulmonary artery-on-a-chip. (a) Schematic diagram of pulmonary vascular remodelling in PAH. (b) α-SMA (red) and vWF (green) staining in healthy and PAH lung. Bar=50μm. (c) BMPR2 mRNA expression in HPAECs treated AdCTRLshRNA with Ad-BMPR2-shRNA-GFP. n=3; **P<0.01;

unpaired t test. (d) Effect of double hit (hypoxia and BMPR2 knockdown, 24h) on HPAEC permeability, measured as passage of 40kDa FITC-dextran (1mg/mL) from top to bottom channel; n=9 individual chips. (e) Effect of hypoxia and endothelial BMPR2 knockdown on HPASMC proliferation (24h, EdU assay). Cells were untreated or were treated with 10μM imatinib mesylate for 24hrs. n=4-5 individual chips. In (d, e) error bars indicate mean ±SEM of a one-way ANOVA with a Tukey's post-hoc correction test. Volcano plots show differentially expressed genes (DEG) in (f) HPAECs treated with BMPR2shRNA, (g) HPAECs in the "double hit" PAH model (BMPR2shRNA and hypoxia), (h) HPASMCs in the "double hit" PAH model. Downregulated genes are in blue and upregulated genes are in red; P<0.05, 0.25-fold cut-off. n=4.

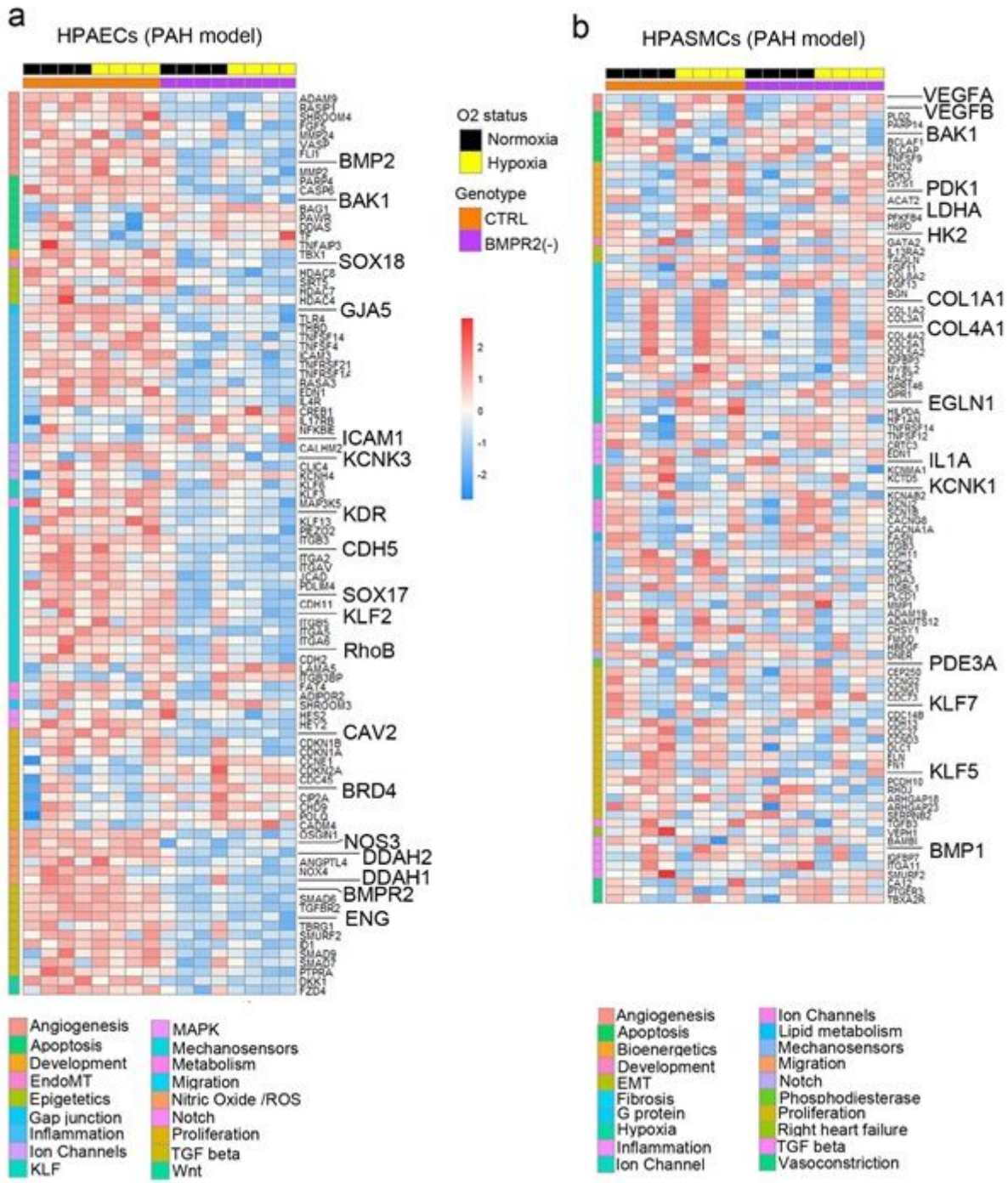

Figure 3

PAH pathways in the “double hit” disease model. Top DEG associated with cardiovascular diseases were grouped into categories and visualised as transcripts per million (TPM) heatmaps. Colour coded pathways are shown underneath the heatmaps, with key gene symbols enlarged in (a) HPAECs and (b) HPASMCs. The genotype status (control and BMPR2 knockdown) and oxygen status (normoxia or hypoxia) are shown at the top of the heatmap in different colours, as indicated. Changes in gene expression are also colour coded, with blue denoting a lower relative gene expression and red denoting a higher relative gene expression. Each column represents 1 experimental repeat (n=4/treatment group).

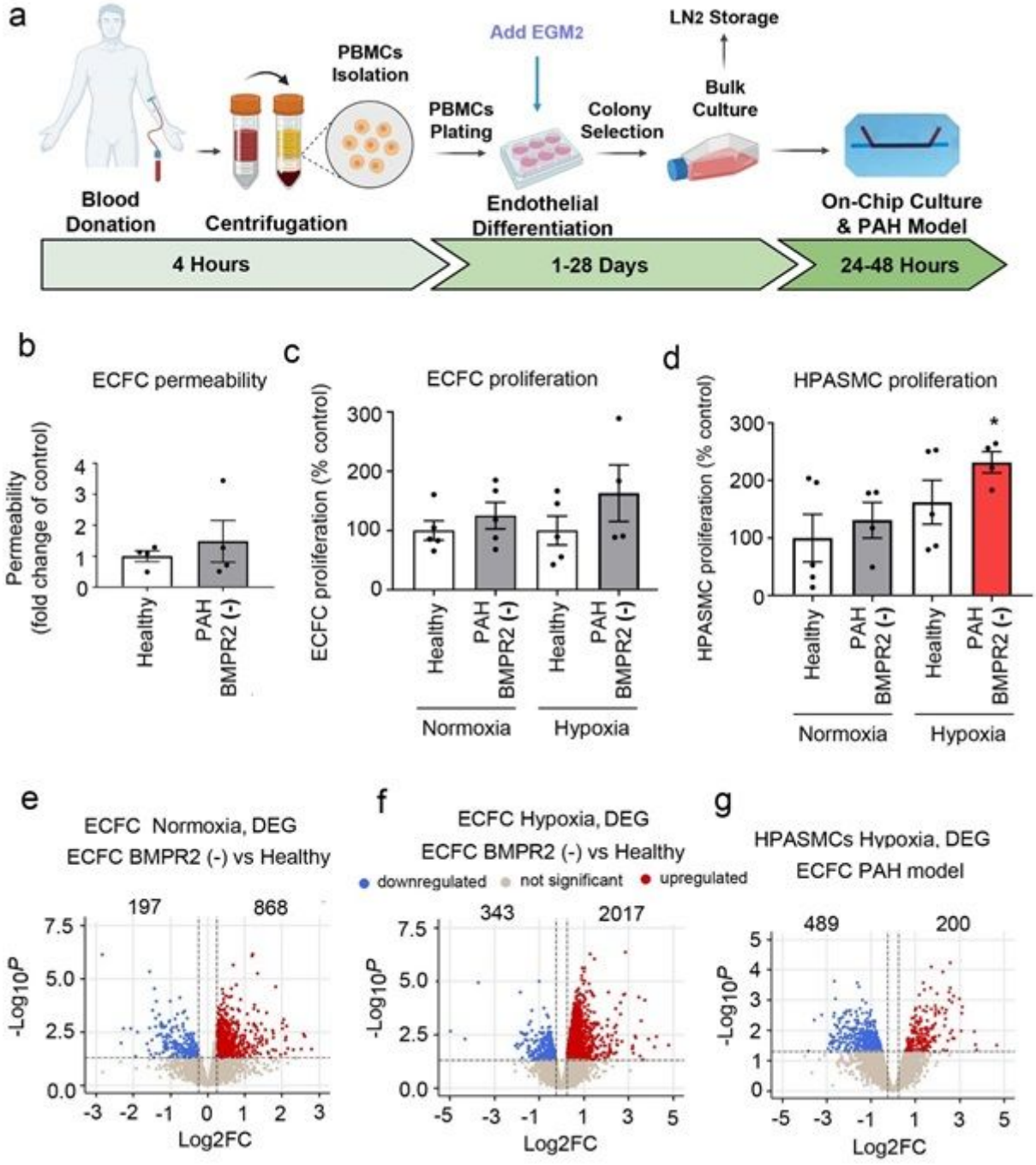

Figure 4

Model validation using cells from PAH patients with BMPR2 mutations. (a) Schematic diagram of isolation and culture of patient ECFCs. (b) Permeability of ECFCs from healthy individuals and PAH patients with BMPR2 mutations cultured in PA-on-a-chip. (c) Proliferation of healthy and PAH ECFCs in PA-on-a-chip under normoxic or hypoxic conditions (2% O2, 24hrs), as indicated. (d) Proliferation of HPASMCs co-cultured with control or patient ECFCs under normoxic or hypoxic conditions. n=4-5 biological donors, each assayed in a separate chip. Bars are means ±SEM; one-way ANOVA with a Tukey post-test; *p≤0.05. Volcano plots show (e) DEG in PAH ECFCs with BMPR2 mutations vs healthy controls in normoxia, (f) DEG in PAH ECFCs vs healthy controls in hypoxia (ECFC PAH model), (g) DEG in HPASMCs in hypoxia. In (e-g) n=5 biological donors, each in a separate chip.

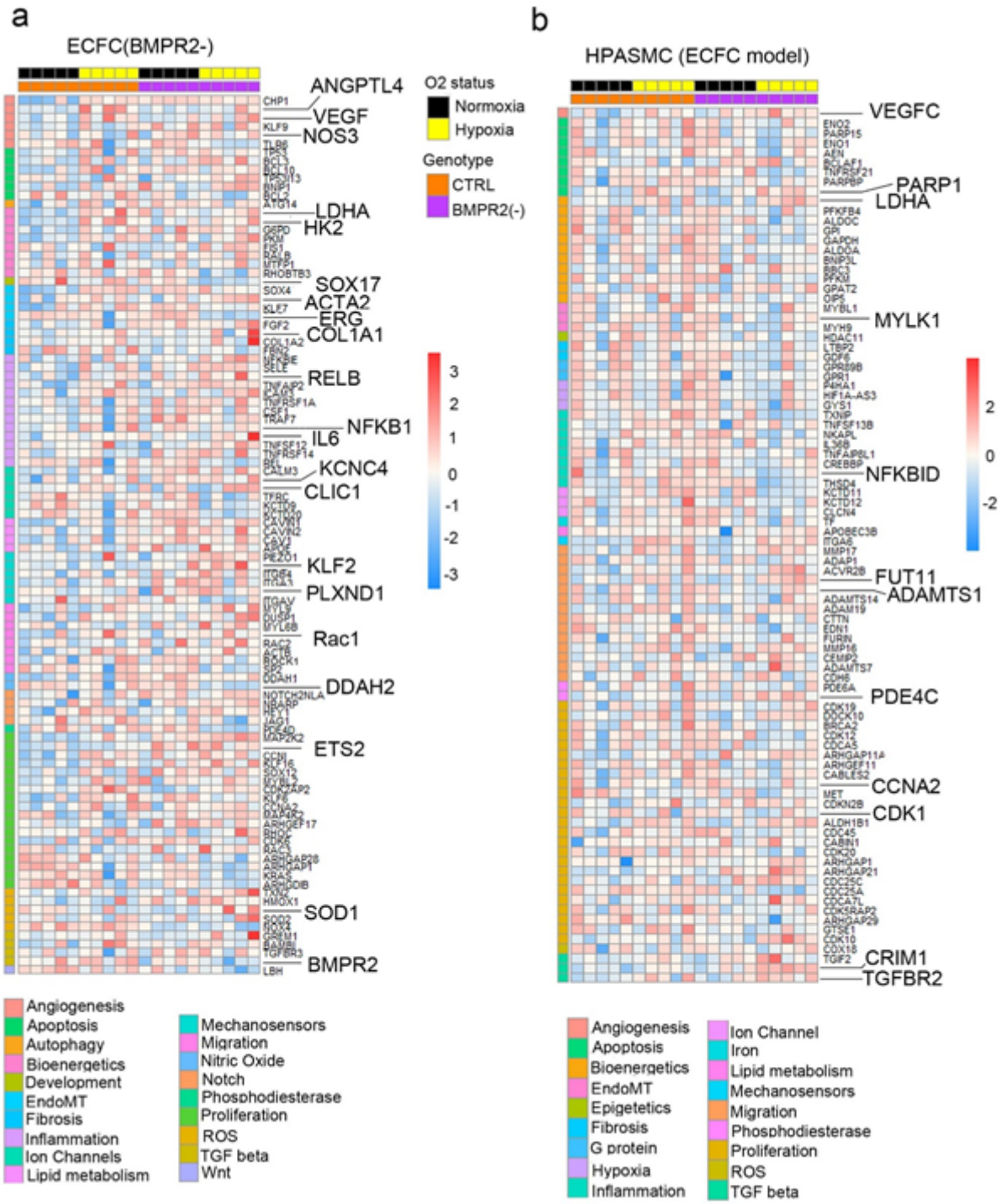

Figure 5

Disease pathways in control and patient-derived ECFC datasets. Top DEG associated with cardiovascular diseases were grouped into categories and visualised as TPM heatmaps. Colour coded pathways are shown underneath the heatmaps, with key gene symbols enlarged in (a) PAH ECFCs and (b) HPASMCs co-cultured with ECFCs. The genotype status (control and BMPR2 knockdown) and oxygen status (normoxia or hypoxia) are shown at the top of the heatmap in different colours, as indicated. Changes in gene expression are also colour coded, with blue denoting a lower relative gene expression and red denoting a higher relative gene expression. Each column represents 1 donor; n=5 different biological donors/treatment group.

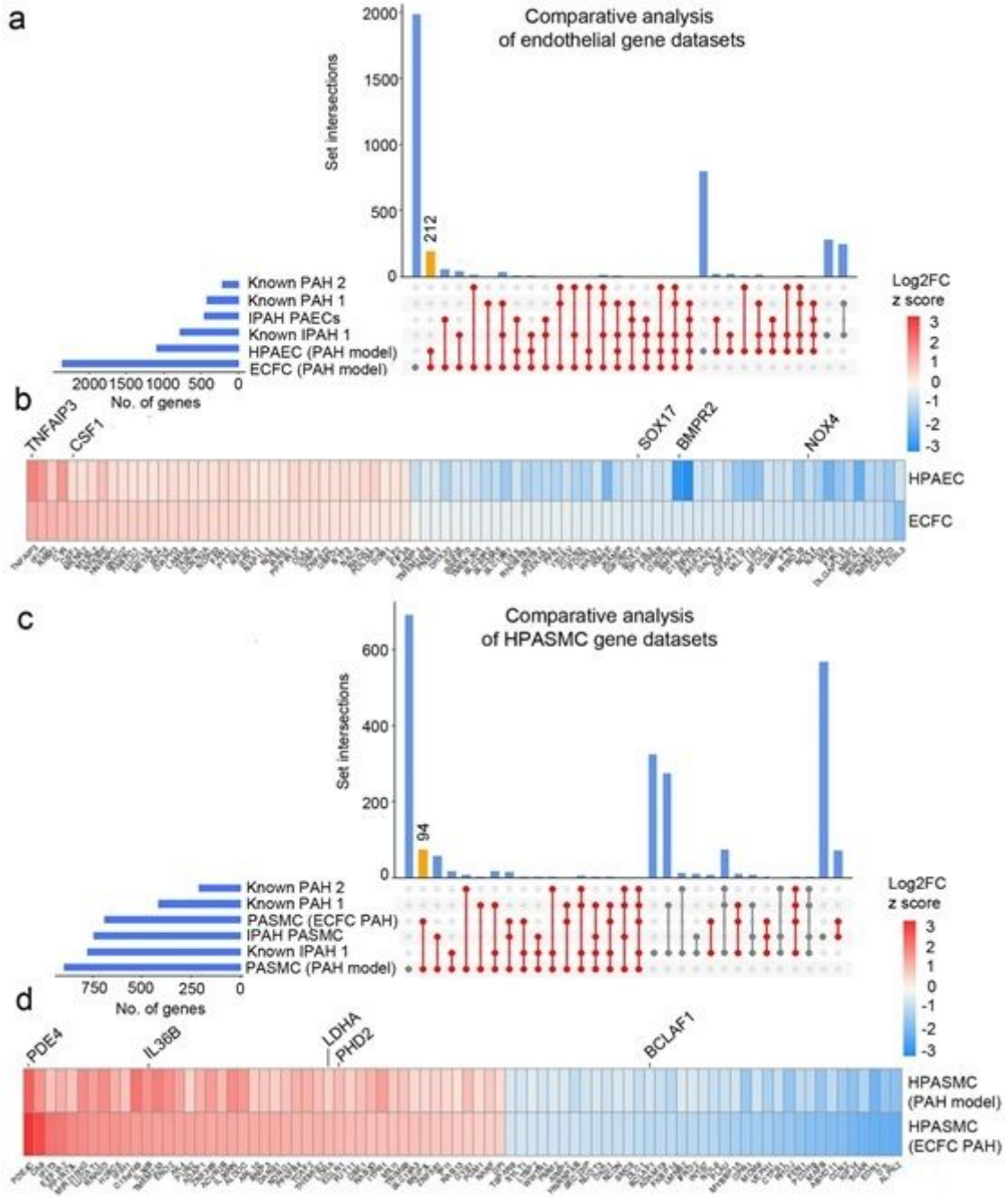

Figure 6

Comparative analysis of microfluidic PAH models and published PAH and IPAH gene datasets. DEG datasets from the adenoviral “double hit” models (PAH Model) and patient ECFC models (ECFC PAH) of PAH were compared against previously reported RNAseq studies and lists of genes known to be associated with PAH and IPAH. UpSet plots and heatmaps detail comparative analysis of (A, B) endothelial gene datasets and (C, D) smooth muscle cell datasets. In (A, C) the largest gene overlaps are highlighted in yellow. Heatmaps in (B, D) visualise similarity of gene expression changes between the two microfluidic models of PAH, the “double hit” PAH-model and the ECFC PAH model; downregulated genes are in blue and upregulated genes are in red. RNAseq datasets used for comparative analysis were from PASMCs from IPAH lung transplants22 (database named here “IPAH PASMC”); PAECs isolated from IPAH lung transplants23; (named here “IPAH PAEC”). Other gene databases with known PAH associations were from 24 and included: Disgenet public website https://www.disgenet.org/search (here named “known PAH1”); DisGENET PAH (https://www.disgenet.org/browser/0/1/0/C2973725/), (here named “known PAH2”); DisGENET IPAH (https://www.disgenet.org/browser/0/1/0/C3203102/) (here named “known IPAH1)

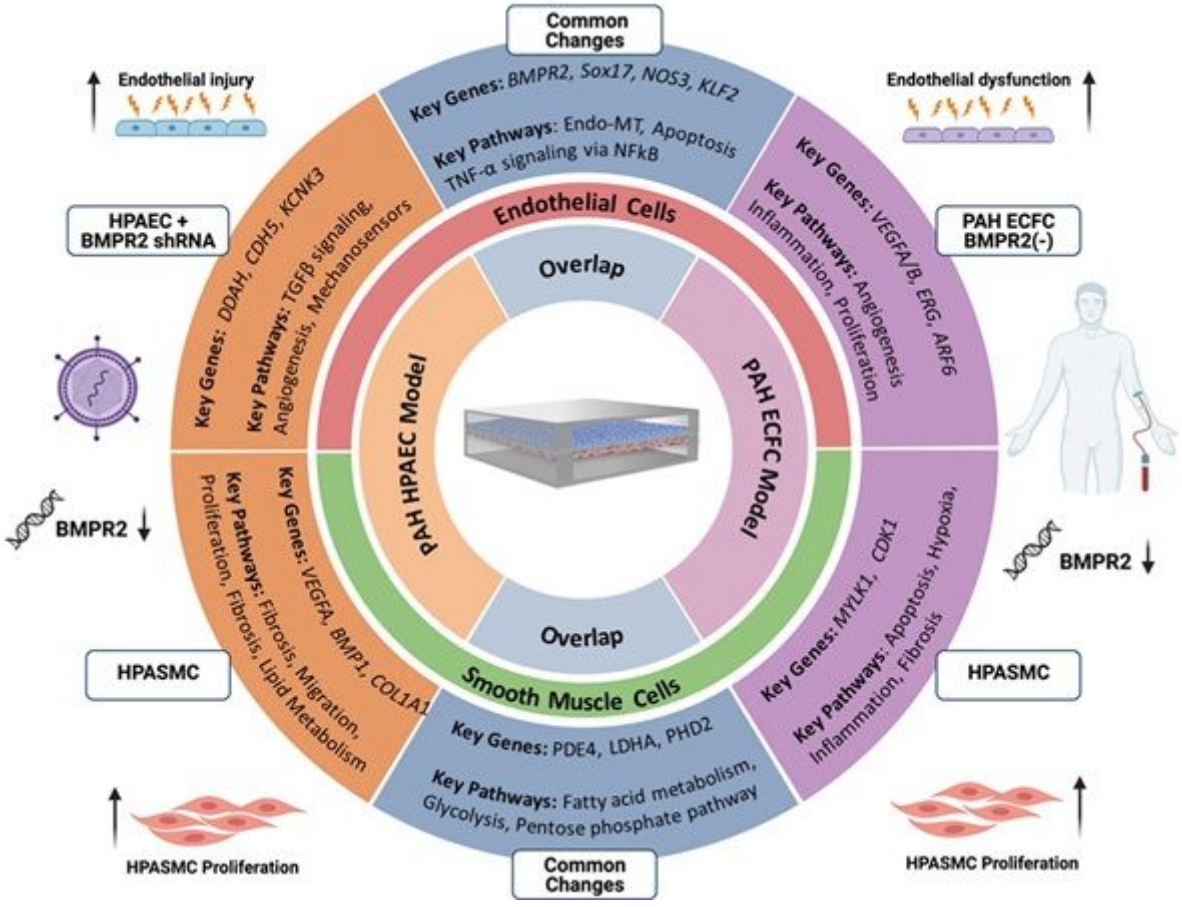

Figure 7

Microfluidic “double hit” model of PAH. AdBMPR2 shRNA-treated HPAECs and PAH ECFCs with disabling BMPR2 mutations were co-cultured with HPASMCs under hypoxic (2% O2) conditions in PA-on-a-chip for 24h. The diagram shows selected key PAH genes and pathways identified by transcriptomic profiling of endothelial and smooth muscle cells.

Supplementary Files

This is a list of supplementary files associated with this preprint. Click to download.

- FileS1ListofDEgenesinDisease.SignaturedoublehitHPAECandECFCmodels.xlsx
- FileS3pathwayanalysisofBMPR2independentgenesinHPAECsdoublehitmodel.xlsx
- FileS2BMPR2independentgenelistindoublehitPAHmodel.xlsx
- FileS4alistofHPAECandHPASMCgenesaffectedbyHPAECBMPR2silencing.xlsx
- FileS5pathwayanalysisofhypoxiainducedBMPR2independentgenesinHPASMCsdoublehitmodel.xlsx
- FileS6alistofoverlappinggenesnormoxicADENOvsECFCs.xlsx
- FileS7listofDEgenesinBMPR2deficientECFCandHPASMCs.xlsx
- FileS8pathwayanalysisofhypoxiainducedgenesinECFCsinthedoublehitmodel.xlsx
- FileS9pathwayanalysisofhypoxiainducedgenesinHPASMCsinthedoublehitECFCmodel.xlsx
- FileS10AllDEdatasets.xlsx
- FileS11overlappinggenelistsfromFigure8.xlsx
- FileS12newHPAECOVERLAPMSIGDBPATHWAYSALL.xlsx
- FileS13HPASMCOVERLAPMSIGDBPATHWAYSALL.xlsx
- MicrofluidicmodelPAHSUPPLEMENT.docx